University of Natural Resources
and Applied Life Sciences, Vienna

Separation of BSA multimers on anion exchange media: chromatographic modelling including extra-column effects

Jürgen Beck, B.Sc.

Master Thesis
in partial fulfillment of the requirements for the degree of

Diplom-Ingenieur

Department of Biotechnology

University of Natural Resorces and Applied Life Science, Vienna

Department Head: Univ.Prof. Dipl.-Ing. Dr. Reingard Grabherr
Supervisor: Assoc. Prof. Dipl.-Ing. Dr. Rainer Hahn

Acknowledgements

I would like to thank my supervisor Rainer Hahn for all the help and valuable input, without which this master thesis would never have been completed.

For their educational and patient introduction to chromatographic modelling and the training I received in using the CADET system, I would like to thank Eric von Lieres, Juliane Diedrich and William Heymann of Forschungszentrum Jülich. The discussions about mixing behaviors and the general capabilities of a system like CADET and the possibilities it provides were eye-opening.

Last but not least I would like to thank all colleagues in my working group for their help in the lab and their unceasing moral support.

Zusammenfassung

In dieser Arbeit wurde die Trennung von BSA Monomer und Multimeren als Modellsystem für die Untersuchung der Einflüsse von Systemvolumina auf die Trennleistung bei Anionenaustauschchromatographie und die Bestimmung der Proteineigenschaften herangezogen.

Auswertung von Isothermen zeigte, dass bei der BSA Ausgangsprobe mit einem Multimergehalt von ∼20% kein Plateau erreicht wird. Reines Monomer zeigte hingegen klassisches Langmuir-Adsorptionsverhalten. Durchbruchsanalysen zeigten, dass die Front von reinem Monomer ein scharfes Profil hatte und rasch Equilibrium erreichte. Die Kurve der Probe mit ∼20% Multimeren zeigte langes "tailing" verursacht durch die Verdrängung des Monomers durch stärker bindende Multimere. Höhere Multimerkonzentration führte zu schnellerem Erreichen des Equilibriumzustands.

Erhöhter Einfluss von Systemvolumina bei kleinen Säulen führte zu einer starken Veränderung von Adsorptionsmodellparametern. Elutionssalzkonzentrationen könnten durch diesen Effekt unterschätzt werden. Die Trennleisung nimmt ebenfalls mit dem Säulenvolumen ab. Chromatographieläufe wurden mit dem "general rate model" und dem "Steric Mass Action model (SMA)" als Adsorptionsmodell und mit BSA Monomer als Probe modelliert. Verschiedene Umrechnungsmethoden von Leitfähigkeit zu Salzkonzentrationen führen zu unterschiedlichen SMA Parameterwerten. Zudem sind die Werte nicht kongruent zwischen numerischer Parameteroptimisierung und Parameterschätzung bei Isothermen.

Simulationen von Gradientenelution bei verschiedenen Steigungen wurden für drei Säulen berechnet. Abweichung von simulierten und experimentellen Werten war dabei unter 10%. Das erstellte Model war zudem fähig das Elutionsprofil von BSA Monomer mit steigender Menge an Probe vorherzusagen. Ein Modell für die Blasenfalle des ÄKTA Pilot wurde erstellt um deren Mischverhalten zu simulieren, nachdem Bandverbreiterung während Stufenelution beobachtet wurde.

Abstract

In this work the separation of BSA monomer from multimers in a crude sample of BSA was used as a model system to investigate the influence of extra-column volumes on separation efficiency on polymeric anion exchange medium and characterization of protein properties.

Isotherm data showed that crude BSA samples containing ∼20% dimers were not of a classic Langmuir-type and did not reach a plateau, whereas pure monomeric BSA exhibited classical Langmuir adsorption behavior. Frontal analysis studies showed that the pure monomeric BSA breakthrough had a sharp profile with rapid achievement of equilibrium. Crude BSA exhibited extreme tailing caused by displacement of monomer by dimer. Higher dimer concentrations in the sample lead to more rapid reaching of equilibrium.

Extra-column effects in small columns were shown to have a large influence on the outcome of retention factor determination. Peak salt concentration would be underestimated when using data obtained from smaller columns. Resolution between species was also shown to be affected by column size. Chromatographic runs were modelled by the general rate model using the Steric Mass Action model (SMA) as adsorption model and pure monomeric BSA as sample. Different methods of converting conductivity to counter-ion concentration result in distinct SMA parameter sets. SMA model parameter determination was found to be inconsistent between numerical parameter optimization and SMA isotherm fitting of batch adsorption data.

Predictions of LGE runs at different gradient lengths were performed for three columns. The deviation between predicted and experimental values for all gradient lengths was below 10%. The model was able to predict the elution profile of BSA monomer with increasing sample loads. A model for the ÄKTA Pilot bubble-trap was created to simulate the mixing behavior during step-elution, after observing band-broadening during step-elution.

Contents

1 Introduction

In the last decades the market for biopharmaceuticals, e.g. monoclonal antibodies, hormones or enzymes has increased exponentially and it continues to grow, with a steady stream of new products entering the market[1]. The ongoing development of new biological therapeutics and increase in manufacturing volume necessitates continuous development of downstream processing. Downstream processing is responsible for the majority of total manufacturing costs in large scale operations [2]. Biopharmaceuticals require extreme purity and a defined composition according to specifications set by regulatory authorities. This includes charge variant and aggregate content. Chromatographic purification steps are the method of choice for downstream processing of proteins, due to very high capture and separation efficiency [3]. Downstream processing development for chromatography steps is often performed with small columns to limit the amount of expended material. Chromatographic modelling of separation processes is a powerful tool to close the gap between experimental results on small columns and prediction of separation in pilot and process scale. Accurate characterization of protein properties and separation characteristics can aid process development and facilitate up-scaling. However it is as yet impossible to accurately predict host cell protein interferences or other irregularities of each individual process. Recently efforts were made to integrate fraction collection and subsequent multi-component parameter optimization to predict peak profiles and design a pooling strategy.[4]. The aim of mechanistic modelling is not to eliminate experiments, but to reduce the amount to a minimum.

In working with small columns it is imperative to consider the contribution of extra-column effects [5]. Chromatography workstation system volumes like buffer mixers, valves and tubings each contribute to extra-column band broadening in a specific way, which is especially large when the column volume is small [6].It is standard practice to characterize a column by performing pulse input experiments with a non-binding tracer to determine the Height Equivalent to a Theoretical Plate (HETP) for the column[7]. This measurement is highly sensitive to extra-column band-broadening [8] with as much as 50 to 80% of total band-broadening being caused by extra-column volumes [9, 10].

The aim of this master thesis was to investigate extra-column volume effects on the separation of a crude BSA sample with a high content of multimers by anion-exchange chromatography. Differences in resolution between monomer and dimer peaks were evaluated for different column sizes. The method of determining retention factors of a protein, developed by Yamamoto et al. [11, 12], discussed in detail in Section 3.2.4, was used as a basis for comparison between columns. Also, the Chromatography Analysis and Design Toolkit (CADET) was used to estimate SMA model parameters for the pure BSA monomer and comparisons were drawn between the different methods of determining the model parameters. Band-broadening contribution of the ÄKTA Pilot bubble-trap was investigated and a model created to simulate mixing behavior. Batch adsorption and frontal analysis experiments were carried out to characterize the crude BSA model system.

2 Theory

2.1 Liquid Chromatography

The term *Chromatography* is used for a variety of separation techniques. The basic concept is that an analyte in a mobile phase is separated from a complex mixture by differential adsorption on a solid phase. The analyte moves slower through the stationary phase than other components of the mixture, which results in a separation based on the favorability of the binding to the stationary phase. The most common type of chromatography is column/packed bed chromatography, where the stationary phase, consisting of porous particles with various properties, is packed into a cylinder with the mobile phase moving from the inlet of the column through the packed bed to the outlet. There are two types of column chromatography which are distinguished by the aggregate state of the mobile phase: gas- and liquid Chromatography. In liquid chromatography the analyte moves through the bed in the mobile phase, enters the particle through a pore and adsorbs on the surface. Depending on the type of chromatography employed, the analyte is either moving slower or faster than other components or remains bound on the stationary phase until eluted or displaced by appropriate means. A detailed discussion of the different modes of operation of column chromatography can be found in [3, 13]. The transport processes occurring in a column during operation can be described by the so-called general rate model.

2.2 General rate model

The General Rate Model (GRM) is a comprehensive model describing mass transfer, ad- and de-sorption processes and axial dispersion in liquid chromatography [14–17]. Molecules are transported through a packed bed in the bulk liquid and move through the *void fraction* ε of the column at the *interstitial velocity* ν. A concentration gradient between the mobile phase in the interstitial space and the liquid in the pores is the driving force for *film mass transfer*, which transports the molecules into the particle. There is no convectional mass transfer acting on the molecule once inside the particle. The transport inside the pore is controlled by diffusion. The type of diffusion that is most prevalent depends on the type of resin and the behaviour of the protein.

There are three types of diffusion inside of a pore: *pore diffusion*, *solid diffusion* and *parallel diffusion* where both pore and solid diffusion are present [3]. Pore diffusion occurs in large liquid filled pores, where no solid phase is impeding the diffusion of the molecule. Solid diffusion occurs when the pores are filled with solid phase in a matrix, in a bound state on the pore surface and in particles with small pores. Parallel diffusion occurs in a mixture of cases e.g. particles with a large distribution of pore sizes [7].

In a packed bed, under real process conditions, molecules are not homogeneously distributed in all dimensions but display *axial dispersion* D_{ax} which lead to band broad-

ening dependent on the diffusivity of the molecule in dilute solution called *free diffusivity* D_0, hydrodynamic dispersion and heterogeneous packing of beads in the column. Radial dispersion is in most cases neglected as a significant influence on the transport behaviour of the protein [3].

In most protein chromatography processes mass transfer is the limiting factor and the contribution of the radial and axial dispersion on band broadening is negligible and thus often omitted from calculations [3].

The general rate model for liquid column chromatography consists of a bulk fluid partial differential equation [16] to describe mass transfer of molecules through the interstitial volume of the column by convective flow, band broadening by axial dispersion and film mass transfer into the particle, described by

$$\frac{\partial c_i}{\partial t} = -\nu \frac{\partial c_i}{\partial z} + D_{ax} \frac{\partial^2 c_i}{\partial z^2} - \phi \frac{3}{r_p} k_{f,i}(c_i - c_{p,i}) \tag{2.1}$$

Here, c_i denotes the concentration of a solute in the bulk fluid, $c_{p,i}$ the concentration of solute in the liquid inside the pore, ν is the interstitial velocity, D_{ax} the axial dispersion coefficient, ϕ the phase ratio, given by $\phi = 1 - \varepsilon/\varepsilon$, where ε is the column void fraction and $k_{f,i}$ the film mass transfer coefficient.

Inside the pore the mass transfer is entirely dependent on diffusion [3]. In this thesis only pore diffusion was considered in modeling of a column packed with particles of the anion exchange resin Source 30Q. Based on experimental results published by Susanto et al. [18] surface diffusion can be neglected as an influence on mass transport inside the pore for this type of resin. The mass balance for the porous particles is given by

$$\frac{\partial c_{p,i}}{\partial t} = D_{e,i} \left(\frac{\partial^2 c_{p,i}}{\partial r_p^2} + \frac{2}{r} \frac{\partial c_{p,i}}{\partial r_p} \right) - \frac{1 - \varepsilon_p}{\varepsilon_p} \frac{\partial q_i}{\partial t} \tag{2.2}$$

where $D_{e,i}$ is the pore diffusion coefficient of the solute, ε_p is the particle porosity and q_i is the concentration of bound solute on the solid phase. In this thesis, rapid equilibrium conditions inside the pore were assumed and expressed by

$$\frac{\partial q_i}{\partial t} = 0 = fads[c_{pi}, q_i] \tag{2.3}$$

The correlation between $c_{p,i}$ and q_i is described by an appropriate adsorption model for the chromatographic method, such as the Langmuir, Stoichiometric Displacement or Steric Mass Action models.

Generally, Danckwerts' boundary conditions [19] are applied to the column inlet Eq. (2.4) and outlet Eq. (2.5) to describe the mass transfer in and out of the column.

$$vc_{in,i}(t) = vc_i(t,0) - D_{ax}\frac{\partial c_i}{\partial z}(t,0) \qquad \forall t > 0 \tag{2.4}$$

$$\frac{\partial c_i}{\partial z}(t,L) = 0 \qquad \forall t > 0 \tag{2.5}$$

2.3 Ion Exchange Chromatography

Ion Exchange Chromatography (IEX) is the most widely used type of chromatography for protein purification [7]. IEX chromatography separates molecules based on their *net surface charge* z. Molecules with different surface charges vary in the degree of their electrostatic interaction with the oppositely charged ligands of the chosen IEXmedium and can be separated based on this adsorption difference in elution chromatography. There are two types of IEX resin: Anion-exchange (AIEX) resins and Cation-exchange (CEX) resins, which are further categorized as weak or strong based on the protonation strength of the used ligand. Proteins are large *amphoteric* biomolecules consisting of a long chain of amino acids with a varying amount of weakly acidic or basic amino acids. Each protein has a specific sequence containing charged amino acids which are influenced in their charge state by the pH of the surrounding environment. At a certain pH value the *net surface charge* will be zero, because no amino acid is in a charged state. This pH value is the *isoelectric point* pI of the protein. The relationship between pH and *net surface charge* is unique for specific proteins. Each protein is either positively or negatively charged depending on the amino acid composition and the surrounding pH. At a pH lower than the pI the protein is positively charged and at a pH higher than the pI the protein is negatively charged.

In an IEX chromatography process the sample solution is applied to the column and the target protein binds *reversibly* to the oppositely charged ligand by electrostatic interaction. The pH of the buffer is selected in a buffer screening beforehand to maximize the binding of the target protein to the resin. All uncharged impurities and molecules with the same charge as the ligand are washed out after the sample loading step. Conversely, the buffer conditions can be optimized for the binding of contaminants and the target protein can be collected in the flow through. Elution of a bound protein is performed by increasing the salt concentration in the mobile phase. The increase in concentration of counter-ions (in most cases Na^+ and Cl^-) slowly displace the proteins, with which they are competing for charged ligands, from the resin. Weakly charged proteins elute at a lower counter-ion concentration than proteins with a higher charge. This is used to separate proteins of the same charge, but with different charge states during linear gradient or isochratic elution. Different adsorption models are available describe the process of protein adsorption to IEX resins.

2.4 Adsorption models

Adsorption models are represent the physical manifestation of adsorption of a molecule, such as a protein, on a stationary phase. Protein adsorption is highly complex and in many cases the adsorption models are insufficient to accurately capture the complexities involved in the binding of a protein to a surface. However, they approximate to a good description of the adsorption process of proteins.

The relationship of molecule concentration in the supernatant and molecule adsorbed on the stationary phase is expressed by the *adsorption isotherm*. The most commonly used adsorption model is the *Langmuir adsorption isotherm* which is applicable for all stationary phases where adsorption follows the classic Type I adsorption shape. For IEX resins, where the adsorption process is characterized by the *protein effective charge* z, the commonly used models are the Stoichiometric Displacement Model (SD) and Steric Mass Action (SMA) model

Langmuir adsorption

The Langmuir adsorption isotherm [20] was originally developed to describe gas adsorption on inorganic surfaces. Nevertheless it is an appropriate model to describe the adsorption behaviour of many proteins and multi-component mixtures, since they often reach a plateau state comparable to the "Langmuir" Type I adsorption shape. Adsorption is assumed to take place in a monolayer until the whole available ligand surface is saturated and in equilibrium with the concentration in the liquid phase.The Langmuir adsorption model is given by

$$q = \frac{q_m K C}{1 + KC} \tag{2.6}$$

where q is the concentration of adsorbed solute, q_m the maximum concentration of adsorbed solute, K the equilibrium constant of adsorption, and C the concentration of solute in the supernatant.

Stoichiometric displacement

The SD model introduced by Kopaciewicz et al. [21] proposes, that the binding of proteins on the stationary phase of an IEX resin is based on a stoichiometric exchange of counter-ions with the surface charge of the protein. These assumptions were used to derive the following following equation

$$q = \frac{K_e(q_0 - zq)^z C}{(C_{Na^+})^z} \tag{2.7}$$

where q is the concentration of solute adsorbed on the stationary phase, K_e the equilibrium constant, q_0 is the total ionic capacity of the used resin, z the effective charge of

the prote.in, C the concentration of solute in the fluid phase and C_{Na^+} is the concentration of counter ions in solution.

The maximum adsorbed concentration q_{max} is given by:

$$q_{max} = \frac{q_0}{z} \tag{2.8}$$

Steric mass action model

The SMA model, proposed by Brooks and Cramer [22], is an extension of the SD model and includes the steric shielding of charges by the protein, caused by its large size in comparison to the ligands. It introduces the *shielding coefficient* σ to include the effect into the isotherm expression of the SD model:

$$q = \frac{K_e[q_0 - (z + \sigma)q)]^z C}{(C_{Na^+})^z} \tag{2.9}$$

with

$$q_{max} = \frac{q_0}{z + \sigma} \tag{2.10}$$

2.5 Linear Gradient Elution

Linear gradient elution (LGE) is regularly used in chromatographic purification of proteins, because of its capacity to separate complex sample mixtures[3]. In practice a sample contains molecules of varying size, adsorption properties and strengths, charge states and charge strengths, which can be used to separate the target protein from impurities present in the mixture.

LGE is performed by loading the sample onto the column, washing out unbound impurities and then introducing a linear gradient of modifier concentration, by mixing the binding buffer with an elution buffer with a high modifier concentration. In IEX chromatography, this results in a separation of proteins according to their charge strength, with the weakly adsorbed proteins eluting first, and the strongly adsorbing proteins later at a higher modifier concentration. This effect is reflected by the SD Eq. (2.7) and SMA Eq. (2.9) adsorption isotherms, where q decreases in the presence of a higher salt concentration. Proteins with a high effective charge z exhibit a higher adsorbed solute concentration at the same salt concentration compared to proteins with a lower z value. This causes them to move at different speeds along the salt gradient in the column, resulting in a separation of the two proteins.

Determination of retention factors by linear gradient elution

Protein retention factors in IEX chromatography, based on the SD model, can be determined by performing linear gradient experiments with varying gradient slopes, with a sample load in the linear range of the isotherm. The parameter estimation is based on the change in peak salt concentration C_M at different gradient slopes [23]:

$$C_M = \left[A(z+1)\gamma - (C_I^0)^{z+1}\right]^{\frac{1}{z+1}} \tag{2.11}$$

in practical applications the contribution of the initial concentration of salt C_I^0 is often neglectable since the target protein binds very strongly at the starting conditions of the separation.

The equation is then simplified to:

$$C_M \sim [A(z+1)\gamma]^{\frac{1}{z+1}} \tag{2.12}$$

where A is a lumped parameter given by

$$A = \phi K_e {q_0}^z \tag{2.13}$$

γ is the linearized gradient slope given by

$$\gamma = \frac{\beta L}{v} \tag{2.14}$$

and β is the gradient slope:

$$\beta = \frac{(C_I^f - C_I^0)}{t_G} \tag{2.15}$$

with C_I^f and C_I^0 being the final and starting concentration of the gradient and t_G the gradient length.

2.6 Modeling extra-column influences on chromatographic processes

All system volumes contribute to the outcome of a chromatographic process [3]. The buffer mixer, connecting tubings, chromatography hardware, valve and detector dead volumes all have a large influence on the final separation result. They contribute to the observed dead volume and effect extra-column peak-broadening. Column evaluation is usually performed by a pulse injection of a non binding tracer. It is necessary to subtract all extra-column influences from the resulting chromatogram to accurately characterize the column performance. In practice this is done by performing a tracer experiment with an empty column system [24] and subtracting the values of the peak first moment and the variance from the results gained by the column evaluation experiment. In IEX chromatography, protein properties are often determined by LGE as described in Section 2.5. Extra-column peak broadening becomes especially important, when the column volume is not sufficiently large to nullify the system volume influence. As previously published by Kaltenbrunner et al. [25] the effects of increased extra-column to column volume ratio are large. For a 1 mL column the extra-column band broadening may be more than 60 % in a tracer experiment. However, a recent paper shows that even on columns with a volume of up to 20 mL extra-column effects may contribute more than 50% to total band broadening [10] with an increase in column diameter being correlated to increase in band broadening due to increased system component volumes and larger intra-column band broadening. Extra column volume also affects the determination of the protein effective charge for IEX chromatography, as will be shown in section 4.

This illustrates the need for accurate system modeling. Determining column or protein properties and parameters without taking into account the system configuration and contribution to the outcome of the experiment can only result in a system specific result, which is only valid on the used workstation. However, if the chromatography setup including the column hardware can be modeled beforehand, the parameter estimation becomes more focused on the actual properties of the colum stationary phase and the sample. When modeling a chromatographic run of a retained compound with a rectangular isotherm it can be assumed, that the pre-column contribution to band-broadening is practically zero, because of the sharpening and concentration of the band at the top of the column. As such only intra-column and post-column dispersion in tubes and dead volumes have an influence on the peak width of an analyte during a separation run.

In practice dead volumes in detectors, valves, mixers and other hardware are generally modeled as a Continously Stirred Tank Reactor (CSTR) [26, 27]. In an ideal CSTR the concentration of a solute leaving the reactor is the same as the concentration in the whole of the reactor at the same time point. This behavior is called *ideal* or *perfect mixing*, where the solute is distributed in the whole tank volume immediately after entering and is uniform throughout the tank at any given time point [28]. In practice perfect mixing is often assumed, since the differences between ideal and non-ideal mixing can often be neglected in process modeling.If non-ideal mixing behaviors are observed, and they lead

to a deviation in outcome, they can be approximated by an appropriate serial or parallel connection of CSTRs correspond to the real Residence Time Distribution (RTD) of tracer in the mixer.

Residence time distribution function of an ideal CSTR:

$$E_{(t)} = e^{\frac{-t}{\tau}} \tag{2.16}$$

Cumulative function:

$$F_{(t)} = 1 - e^{\frac{-t}{\tau}} \tag{2.17}$$

Results of modeling chromatographic separations on columns and membranes including these extra-column system models are promising [26, 27, 29].

Connecting tubes between the system and the column are realized as either a Laminar Flow Reactor (LFR), a Plug Flow Reactor (PFR) or with added axial diffusion as a Dispersive Plug Flow Reactor (DPFR).Since the influence of axial diffusion is neglectable in protein chromatography applications, because of the low diffusion coefficients of most proteins, it is generally modeled as a PFR. The liquid inside tubings exhibits a laminar flow, which is a non-ideal version of a plug flow, where the outer fluid layers are slower than the inner layers resulting in a parabolic flow profile, rather than a plug flow with a straight edge profile [28]. A perfect PFR is used to introduce system delay volume, where no mixing occurs, into the model.

RTD for a perfect PFR:

$$\tau = \frac{V}{Q} \tag{2.18}$$

2.7 Chromatography Analysis and Design Toolkit

CADET is a complete toolkit for modeling packed bed chromatography applications, which was developed at the Research center Jülich [16]. The GRM solver uses spatial discretization to split a column into parts and particles into shells with finite volumes, which makes it possible to express a Partial Differential Equation (PDE) as a large set of Ordinary Differential Equations (ODE) which are faster to compute. The developmental version used for creating the simulations in this master thesis not only includes the open source solver for iterations of the GRM with various adsorption isotherms, but also a more general process simulator. Modeling of extra-column volumes can be included in the chromatographic simulation by connecting simple or complex unit operations before or after the column. The simplest case is a model where the buffer is mixed in a CSTR and connected to the column with a PFR. Connection possibilities are unrestricted, because the network of unit operations is based on graph theory, where one unit operation represents one node which can be connected to any number of other units, provided the mass balance of the system remains unchanged [30]. Once a system is modeled, chromatography columns can be programmed individually and easily connected provided characterization of the workstation was accurate. An example for such a setup is pictured in Fig. 1. This modular setup makes it possible to investigate non-standard peak profiles by introducing specially designed adsorption isotherms to describe the observed behavior as was evidenced by Diedrich et al. by introducing a multi-state steric mass action model to describe a peculiar high loading behaviour of IgG on an IEX tentacle resin [31].

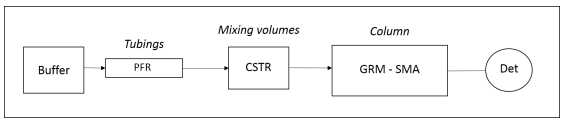

Figure 1: Example for a modeling setup

Parameter optimization

The developmental version used also includes the possibility of optimization for several adsorption model and unit operation parameters. CadetMatch is based on a programming interface written in Python 3, which accesses the CADET engine to create a simulation with a parameter set and an evolutionary algorithm called Strength Pareto Evolutionary Algorithm 2 (SPEA2) [32] for selecting an optimal parameter set with matches the experimental data. Fitting of adsorption parameters is complicated by the fact that the parameters are closely related in effect on the peak shape and position. In such a case a simple gradient algorithm, which can be imagined as working like chemotaxis in bacteria, is not very helpful since there is no single solution to which all other parameter sets converge at the end.

Evolutionary algorithms mimic the way biological organisms are selected for survival by nature. It introduces a number of parameter sets, called a population which each represent a single simulation. Each population produces simulations where the ones best matching the experimental data are selected for reproduction in the next optimization round. Reproduction takes place by mating the selected parameter sets with each other creating hybrid sets which are again selected for survival in the subsequent round. The scoring system implemented in CadetMatch assigns a match score which marks the closeness of the fit to experimental peak shape and position on the time axis. After selection of the highest scoring populations the next generation of parameter sets is produced and evaluated. This process continues until a preset generation number has been reached or a population's score reaches a user defined score percentile.

3 Materials and Methods

3.1 Materials

Protein Sample

Heat precipitated crude BSA with a purity of $\geq 98\%$ was purchased from Sigma Aldrich (order number: *A9647*). This BSA preparation was chosen specifically for its high amount of multimers and other impurities.

3.1.1 Chromatography

All chromatographic runs and adsorption experiments were performed with 20mM Tris/HCl pH 7.5 as running buffer and a 20mM Tris/HCl with 1M NaCL at pH 7.5 as elution buffer. Columns were regenerated with 0.1M NaOH solution and were stored in 20% ethanol, when not in use. Determination of total ionic capacity was performed with a 0.5M solution of $NaNO_3$. Sterile filtered reverse osmosis water was used for preparing all buffers and solutions.All chemicals were purchased from Sigma Aldrich at analytical purity grade. Table 1 shows a list of all columns used in the genesis of this master thesis. Source 30Q (*GE Healthcare*) is a monodisperse, strong anion exchanger with a very high separation efficiency. It was chosen because of it's ability to separate BSA into monomer and dimer peaks.

Table 1: List of all columns used for experiments

Column volume (mL)	**Resin**
630	
40	
6	Source 30Q
1	
0.5	
7.5	Source 15Q
1	Mono Q

Laboratory scale

Laboratory scale experiments were carried out on an ÄKTA Explorer 100 chromatography system from GE Healthcare. Columns were packed with Source 15Q and Source

30Q. Additionally a prepacked Mono Q 5/50 was purchased.

Pilot scale

Pilot scale experiments were carried out on an ÄKTA Pilot system from GE Healthcare. Experiments were performed on a Fineline 100 column packed with Source 30Q resin. For investigation of mixing inside the bubble-trap the elution buffer was colored with Vitamin B12, purchased from Sigma Aldrich.

3.1.2 Analysis

Analytical size exclusion chromatography

A Waters Alliance e2695 High-Performance Liquid Chromatography (HPLC) system was used to perform analytical Size Exclusion Chromatography (SEC) runs on a Superdex 200 Increase 10/300 column (GE Healthcare). Phosphate-buffered saline (PBS) was used in sample dilution and as a running buffer. The chemicals used to prepare standard PBS were purchased from Sigma Aldrich at analytical grade.

UV-Vis spectroscopy

UV-Vis spectroscopy was performed on a Cary 60 photometer from Agilent Technologies. Quartz cuvettes with a path length of one cm were used for measurement.

SDS PAGE

The following table shows all materials used for gel electrophoresis.

Table 2: SDS PAGE reagents

Type	**Name**
Electrophoresis gel	NuPAGE™4-12% Bis-Tris
Sample buffer (2x)	2.5 mL 0.5M Tris-HCl, pH 6.8 + 2.0 mL Glycerin + 4.0 mL SDS 10% (w/v) + 0.5 mL bromophenol blue 0.1% (w/v) filled to 10 mL
Running Buffer (10X)	Tris/Glycine buffer 116 g Tris + 576 g glycine + 40 g SDS in 4 L water
Fixing solution	50% EtOH, 10% acetic acid
Staining solution	Aliquot mixture of 4 parts 0.2% (m/v) coomassie brilliant blue R250 and 3 parts bismarck brown in 40% EtOH, 10% acetic acid
De-staining solution	25% EtOH, 8% acetic acid
Protein ladder	SeeBlue™Plus2 pre-stained protein standard
Hardware	
Electrophoresis system	XCell SureLock™

3.1.3 Software

Peak and curve fitting was done using PeakFit v4 and TableCurve2D v5 (*Systat software*. Graphs were generated with SigmaPlot version 13.0 (*Systat software*). Modelling and parameter fitting was performed with a developmental version of CADET running on Python 3. Visual Studio 17 (*Microsoft*) was used for interface programming and setup of parameter fitting and forward simulations. All other calculations were performed using Microsoft Excel.

3.2 Methods

3.2.1 Chromatographic runs

All chromatographic runs were performed with the same buffer system consisting of an equilibration buffer 20 mM Tris/HCl pH 7.5 and an elution buffer 20 mM Tris/HCl 1M NaCl pH 7.5 . The equilibration buffer was also used as binding buffer for all samples. LGE runs were performed by applying a defined sample volume to the column. A wash step of minimum one column volume with equilibration buffer was performed to wash out all impurities, before the gradient was applied to the column. After the gradient had completed, a clean step with 100% elution buffer was applied for a minimum of 1 CV to remove all molecules still bound to the resin. Then, a re-equilibration step was used to remove the salt from the column. Columns were sterilized with 0.1 M NaOH and stored

in 20 % ethanol. Frontal analysis was performed by equilibrating the column for up to three column volumes, or until UV and conductivity signals were stable. Then, the sample was applied by a step input until the plateau was reached, then the sample was washed out and eluted by step elution with elution buffer until all proteins and other impurities were removed. The column was re-equilibrated sanitized with 0.1M NaOH and stored in 20% ethanol. All runs were performed at a residence time τ of three minutes.

3.2.2 SDS PAGE

Sample preparation for the electrophoresis run was performed by diluting the sample with sample buffer to give a final concenration of $\sim$ 15 µg / 20 µL and incubating for 10 minutes at 95 ° C. The XCell SureLock™running chamber was filled with the running buffer. Then, 20µL of the sample assays and 5 µL of the protein ladder were pippeted into wells. Gel electrophoresis was performed for 2 hours at 200 V with a current of 200 mA. After the runs were completed the gels were immediately put into fixing solution for 30 minutes. The fixing solution was decanted and staining solution was applied to the gel and incubated for 15 minutes. After the incubation period the gel was put into de-staining solution until the colored protein bands were clearly visible against the background. The gel was washed in RO-H_2O for 15 minutes before scanning.

3.2.3 Fractionation

Fractionation of crude BSA sample was performed using LGE. For composition analysis by SDS Poly-Acrylamide Gel Electrophoresis (SDS-PAGE) a very flat gradient was applied to achieve maximum separation. Fractionation was performed on a 40mL Source 30 Q column to obtain pure BSA monomer and a fraction with high dimer content for batch adsorption experiments. A large volume of sample was needed to perform breakthrough curve analysis. This was carried out in pilot scale on a 630ml Source 30Q column. Table 3 shows a list of the used columns and the later usage of the produced samples.

Table 3: List of columns used for fractionation runs

SDS-PAGE			
Column volume (mL)	Resin	Gradient Length (CV)	Sample load (mg per mL column)
7	Source 15Q	50	10

Batch adsorption isotherms			
Column volume (mL)	Resin	Gradient Length (CV)	Sample load (mg per mL column)
40	Source 30Q	30	15

Frontal analysis and LGE			
Column volume (mL)	Resin	Gradient Length (CV)	Sample load (mg per mL column)
630	Source30Q	30	15

3.2.4 Analytical Size Exclusion Chromatography

SEC analysis was performed on a Waters Alliance e2695 HPLC system using a Superdex 200 Increase 10/300 with isocratic application of PBS at a flow rate of 0.5 mL/min. Injection volume of all samples was 100µL diluted to a concentration of $\sim$ 0.1 mg/mL.

3.2.5 Determination of isotherm

Batch adsorption experiments were carried out for crude BSA sample, pure monomer and a sample containing $\sim$ 60% dimer. Batch adsorption was performed using 50% slurry of Source 30Q resin in 20mM Tris/HCl buffer with 16, 40, 64 and 107 mM counter-ion concentration respectively. Buffers were prepared by adding 2.5, 5 and 10% (v/v) 20 mM 1 M NaCl buffer to one part of equilibration buffer. The counter-ion concentration of the equilibration buffer was calculated using the Henderson-Hasselbalch equation (pKa of Tris = 8.1):

$$pH = pK_a + log_{10}\left(\frac{[A^-]}{[HA]}\right) \tag{3.1}$$

Sample concentration was fixed and increasing amounts of slurry were added to the adsorption mixture. The samples were incubated on a rotary mixer overnight at room temperature. Absorption of supernatant was measured with UV-Vis spectroscopy and

the BSA concentration calculated using the Beer-Lambert law and the molar extinction coefficient of BSA monomer.The adsorbed concentration of BSA on the stationary phase, correcting for extra-particle volume, was calculated and the isotherms plotted.

3.2.6 Determination of retention factors

Linear gradient experiments were performed for the crude BSA sample and the purified monomer.It was not possible to achieve discernible separation between variants in samples with concentration of $\geq 50\%$ dimer.

By performing a log transformation on Eq. (2.12) a linear regression can be applied to a log/log plot of C_M/γ:

$$log\gamma \sim C_M(z+1) - log(A(z+1)) \tag{3.2}$$

where the effective charge z is given by the slope $z+1$ and parameter A by the y-axis intercept $-log(A(z+1))$. The obtained parameters can be used to predict the peak salt concentration, and thereby the retention time of the protein in a linear gradient elution.The list of columns used for the crude BSA sample is given in Table 5. Monomer runs were performed using columns listed in Table 4. Peak salt concentrations were calculated by linear interpolation between the measured conductivity of the equilibration and running buffer and their respective counter-ion concentrations.

Table 4: LGE runs BSA Monomer

Column volume (mL)	Resin	Gradient Length (CV)	Sample load (mg per mL column)
40	Source 30Q	1 2 5 10 20 30 50	0.5
6	Source 30Q	1 2 5 10 20 30 50 75	0.5
1 0.5	Source 30Q	2 5 10 20 30 50 75 100	0.5

3.2.7 Influence of bubble-trap on elution chromatography

Linear gradient elution and step elution was performed on the 630 mL Source 30Q Fineline 100 column with and without the bubble trap to evaluate the influence on resolution and band broadening at analytical loads.

3.2.8 Calculation of Resolution

LGE experiments suggested, that there are monomer charge variants present in the crude BSA sample, which result in peak broadening. Peak fitting with PeakFit resulted in numerically acceptable fits, but unlikely distribution of peak areas. Therefore an alternative was chosen based on statistic properties of a Gaussian peak. At 85% peak height the standard deviation of a Gaussian peak is 1.14σ [33] as seen in figure 2. The monomer and multimer peaks were normalized and the peak width at 85% was recorded. The base width of the peak was taken as 6σ and the following formula used to calculate the relative resolution:

$$R_s = \frac{t_{r,2} - t_{r,1}}{\frac{1}{2}(6(\sigma_1 + \sigma_2))} \tag{3.3}$$

where R_s is the chromatographic resolution, $t_{r,i}$ is the respective retention time, and σ_i the standard deviation of the Gaussian peak.

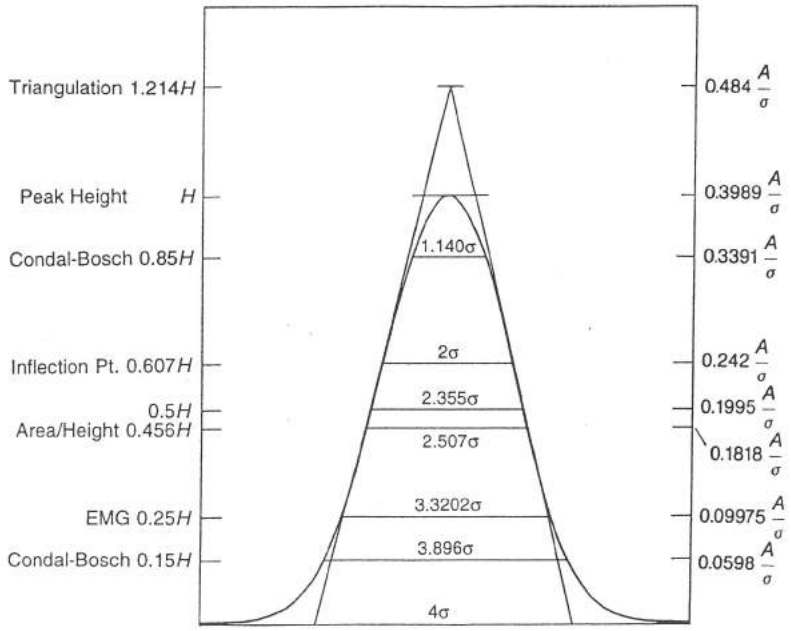

Figure 2: Dimensions of a Gaussian peak

Resolution was calculated for all runs with adequate separation between monomer and dimer. A list of all columns and gradient lengths for which the runs were performed is found in Table 5 below.

Table 5: List of columns and LGE method parameters, gradient length is nominal to 100%B

Column volume (mL)	Resin	Gradient Length (CV)	Sample load (mg per mL column)
6	Source 30Q	1.5 2.5 5 10 20 30 50 75	1.5
1 0.5	Source 30Q	2.5 5 10 30 50 75 100 125	1.5

Determination of pore diffusivity

In order to determine the effective pore diffusivity D_e of BSA pulses were applied to the 6 mL Source 30Q column, at non-binding conditions (20mM Tris 1M NaCl pH 7.5), with increasing flow rates. Increase in flow rate leads to a decrease in mass transfer in and out of the particle, which is reflected as a broadening of the BSA peak and quantifiable as steadily increasing HETP values. The reduced velocity was plotted versus the reduced HETP, whose slope is equal to the slope of the c-term in the van Deemter equation, since the band broadening is entirely mass transfer controlled [7]. This linear regression was used to determine D_e for the protein according to the following equation for the slope:

$$slope = \frac{1}{30}\frac{1}{(1-\varepsilon)}\left(\frac{V_R - V_0}{V_R}\right)^2\left[\frac{10}{Sh} + \frac{D_0}{D_e}\right] \tag{3.4}$$

3.2.9 Frontal analysis

Breakthrough experiments were performed for crude BSA, pure monomer and a mixture containing 50% dimer/multimer, which were obtained by pilot scale fractionation. All experiments were carried out on a 6 mL Source 30Q column. Residence time for all experiments was three minutes. The obtained curves were normalized to bypass absorption values. Curve fitting was performed by fitting the data to a curve calculated using the shrinking pore model with the constant pattern solution of Weber and Chakravorti [34].

3.2.10 Column characterization

Column packing evaluation / Bed porosity ε_b

Column performance evaluation was performed in laboratory scale by injecting a 0.8 M NaCl pulse onto a column equilibrated with 0.4 M NaCl solution. The resulting peaks were then fitted with PeakFit and the asymmetry and HETP were calculated according to the moment theory method for Exponentially Modified Gaussian (EMG) peaks described in *Protein chromatography* chapter 8 [3].Packing evaluation of the pilot scale column Fineline 100 was performed by a breakthrough experiment. The curve was fitted with TableCurve2D using the cumulative EMG function and calculating the first and second moment as described in [25].

System dead volume between detectors

The delay between the UV and conductivity detectors was found to be a very influential factor for the accurate determination of peak salt concentration and subsequently for retention factor calculation using model described in Eq. (3.2). $NaNO_3$ pulses were used to generate salt and UV peaks by injection in the bypass. The conductivity and absorption peaks were fitted separately and the difference in the first moment was taken to be the dead volume between UV and conductivity detector.

Dead volume of column system

A NaCl tracer pulse was injected onto an empty column and the resulting peak was fitted using PeakFit. The first moment was taken to represent the absolute volume between injection valve and the detector.

Void fraction ε

Pulses of plasmid DNA were injected under non-binding conditions ($\geq$ 1M NaCl). The resulting peak was fitted using peak fit, the first moment was taken, the column dead volume subtracted and the result divided by the measured column volume. The void fraction was determined for the 40 mL and 6 mL Source 30Q columns and found to be identical. The obtained values were assumed to be similar for all column sizes.

Particle porosity ε_p

Particle porosity was determined by calculation from the void fraction and bed porosity, determined by plasmid DNA and salt pulses respectively, using the following equation [7]:

$$\varepsilon_b = \varepsilon + (1 - \varepsilon)\varepsilon_p$$

Total ionic capacity

The total ionic capacity was measured for the Source 30Q resin. Pulses of 0.5M $NaNO_3$ solution were injected into the bypass and the absorption at 280nm was recorded. The obtained peak area in mAU/mL was used as a calibration for the determination of the ionic capacity. A 6mL Source 30Q column was saturated with 0.5M $NaNO_3$ solution, washed with water until the conductivity and absorption values were constant. Then the NO^{-}_{3} was eluted with a 1M NaCl solution and the resulting peak area is equal to the saturation concentration of nitrate on the column. The total ionic capacity in mM/mL particle was then calculated by dividing the total nitrate concentration by the column volume minus extra-particle volume. It was determined to be 160 mM/mL resin.

3.2.11 Modelling

Modelling of extra column volumes

ÄKTA Explorer 100 and ÄKTA Pilot system dead volumes were modeled as a series of PFR and CSTR. Where possible measured values were introduced into the modelling of the system, such as the buffer mixer volume. To model the bubble trap of the ÄKTA Pilot, a video was recorded of step input experiments with 20mM Tris/HCl 1M NaCl solution colored with vitamin B12. The recording was examined to determine the mixing behavior inside the bubble trap at different flow rates. The results were used to express the physical realities of the mixing into a model composed of CSTRs.

Chromatographic modelling

The measured column and BSA monomer properties and system model was used in CADET to create a chromatography setup which approximates the real workstation. Parameter fitting with CadetMatch was still being refined at the time of writing. It was therefore not possible to accurately fit both monomer and dimer peak simultaneously to obtain values for SMAmodel parameters, because of low resolution between the two peaks. Parameter estimation was only performed for BSA Monomer. SMA model parameter estimation with CadetMatch is performed by the inverse method described by Osberghaus et al. [35]. The protein effective charge z and the shielding coefficient σ were fitted as discrete values. A LGE run with a gradient from 0-40% B over 4 CV (nominal for 0-100%B over 10CV) was chosen for parameter matching, since there was no visible band broadening due to a possible charge variant. The absorption and conductivity curves were converted to concentration in mM for BSA and counter-ion concentration. The conversion for conductivity curves was done by linear interpolation. There was a discernible discrepancy between the percentage values of the gradient end of 40%B in mS/cm and percentage of elution buffer added, because the relation between concentration and conductivity is increasingly non-linear at higher concentrations of salt [36]. Therefore, it was deemed necessary to perform the parameter fit for two different conversion types. Fits were performed using linear interpolation normalized

to the conductivity of 100% elution buffer and 40% elution buffer. The obtained SMA parameters were used to perform forward simulations to determine the theoretical peak salt concentration of BSA monomer on other column sizes and with different gradient slopes. These values were then compared to the experimental results. It is important to note, that the differences are inconsequential in prediction of peak salt concentration in conductivity, if the same method of linear interpolation is used for conversion. However, SMA model parameters and counter-ion concentration at peak maximum are affected, if the disparity between conductivity and concentration is not accounted for.

Matching peak areas are very important for the parameter optimization process. Experimental chromatograms have to be converted to sec and mM, because CADET exclusively supports SI-Units. Absorption curves were converted by first calculating the concentration of sample applied to the column in mmol/L. A simulation was performed with CADET using this theoretical sample concentration loaded onto the column with a defined flow rate for the amount of time necessary to obtain the equivalent of the sample load in mg/mL. The resulting peak was integrated using PeakFit. The area of the experimental peak was also determined using PeakFit. Next, a conversion factor from mAU/sec to mM/sec was calculated by dividing the peak areas. Finally, the experimental curve was converted to mM using the aforementioned factor.

4 Results

4.1 Experimental characterization

4.1.1 BSA Separation

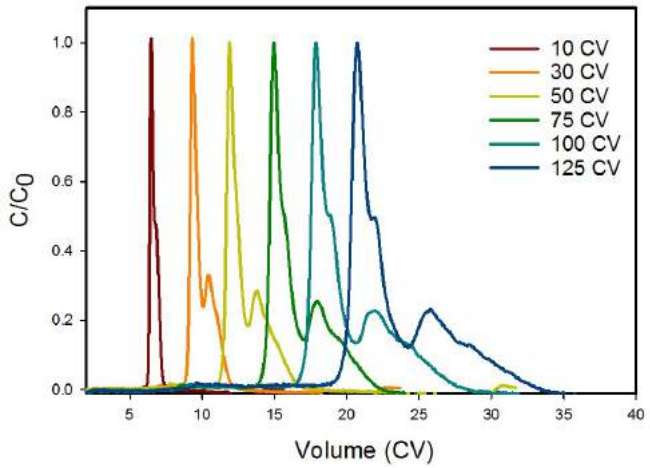

Figure 3: Separation of crude BSA on 1 mL Source 30Q column with increasing gradient lengths, sample load 1.5 mg/mL

Figure 3 shows the chromatographic separation of crude BSA into two protein species on a 1 mL Source 30Q column obtained by LGE runs with increasing gradient length. Separation of species occurs only at shallow gradient slopes. At extremely long gradient lengths there is shoulder formation on the first peak, which could be caused by a charge variant and a gradual widening of the second peak which suggests the presence of more protein variants in the sample.

4.1.2 Model System - BSA characterization

To identify the precise composition of the sample a fractionation run with a very shallow gradient was performed on a Source 15Q column to achieve a higher resolution between the sample components. Sample analysis of the crude BSA sample was performed by collecting fractions during a LGE chromatography run, which were analyzed by analytical SEC and SDS-PAGE as outlined in Section 3.2. Linear gradient elution was performed using a 7.5 mL Source 15Q column with a sample load of 10 mg/mL, because higher resolution was desired. Elution was performed with a 50CV salt gradient Figs. 4 and 5.

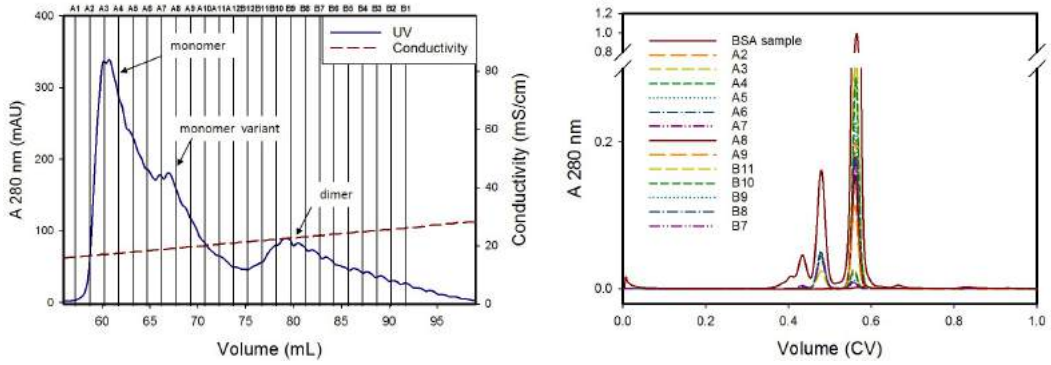

(a) BSA Fractionation (b) SEC Analysis

Figure 4: Determination of sample composition of crude BSA

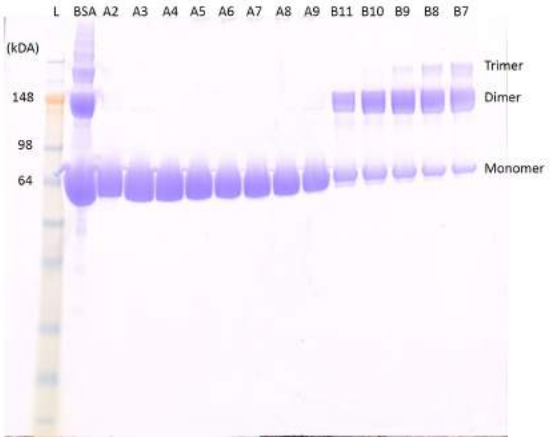

Figure 5: SDS-PAGE of BSA sample and collected fractions

Peak integration of the SEC analysis run of the crude BSA sample showed a sample composition of 78% Monomer, 16% dimer and 6% multimers, based on peak area percentage. Figure 5 shows, that the original BSA sample contains mostly BSA Monomer at $\sim$ 66kDa with the second largest band being the dimer at approx. 130kDA and aggregate variants with high molecular weight, which only represent a small fraction of the sample. Fractions A2 to A9 contain pure monomer as evidenced by Figs. 4 and 5. The peak shoulder is most likely caused by a monomer charge variant. Fractions B11 to B7 show the BSA dimer bands at approximately 130kDA and a steady decrease in monomer content. There is also a low concentration of trimer present in the later fractions.

4.1.3 Separation on different columns

4.1.3.1 LGE with crude BSA

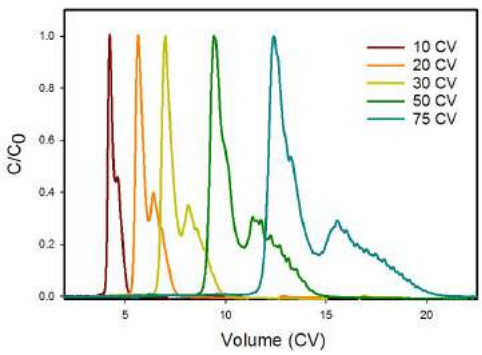

(a) 6 mL column

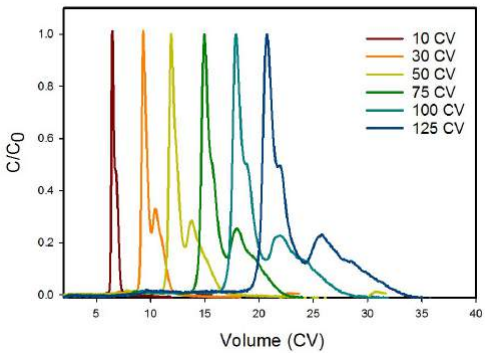

(b) 1 mL column

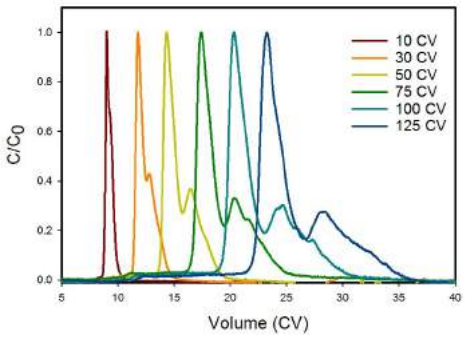

(c) 0.5 mL column

Figure 6: LGE runs of crude BSA with increasing gradient lengths on different columns

LGE runs with varying gradient lengths (see Table 5 in the materials and methods section) of crude BSA were performed on 0.5, 1 and 6 mL Source 30Q columns (Fig. 6) to identify the influence of the columns size on separation of crude BSA. Sample load for all runs was 1.5 mg/mL column volume. It appears that with larger column volumes a smaller gradient length can be used to achieve the same separation as for smaller columns. At a gradient length of 75 CV a monomer variant shoulder is recognizable for the 6 mL column. The monomer variant is barely separating from the main monomer peak of the 1 mL column separation and no shoulder is visible for the 0.5mL column. A more detailed discussion of the resolution is found in Section 4.1.3.2. The peak salt concentration was recorded for the monomer and the dimer peak for all separations to determine the retention factors of the components (see Section 4.1.3.3.

4.1.3.2 Resolution

LGE runs with varying gradient lengths (see Table 5) of crude BSA were performed on 0.5, 1 and 6 mL Source 30Q columns (Fig. 6) to determine the resolution between monomer and dimer peak. Sample load for all runs was 1.5 mg/mL column volume. Calculation was performed as described in Section 3.2.8. It has to be kept in mind that the extremely shallow gradients also contribute to band broadening thus reducing resolution.

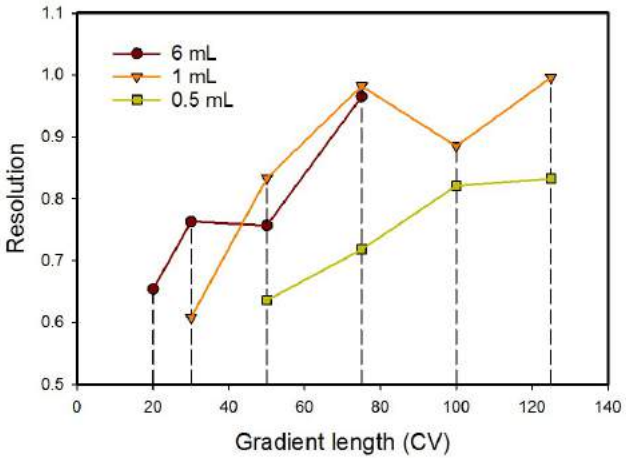

Figure 7: Comparison of Resolution values of crude BSA on different columns with increasing gradient length

Figure 7 shows the difference in resolution of the different column sizes on the same chromatography workstation. The starting point of each line is the first gradient length where the separation between monomer and dimer peaks was sufficient to perform the resolution calculation. This illustrates the difference between the columns with the 6 mL column having sufficient resolution at a gradient length of 20 CV compared to 30 and 50 CV for the 1 mL and 0.5 mL column respectively. The resolution seems to approach a value of $Rs =\sim 1$ for the 1 mL column at the maximum gradient length of 125 CV. This resolution is never achieved for the 0.5 mL column, which stops at a value of ~ 0.8 . Increased width of the peaks at shallower gradients contributes to the stagnation of resolution that is observed in Table 6. This peak broadening could be caused by extra-column effects, by increased separation of charge variants of the sample and the inherent dispersion at high retention volumes. The calculated resolution values in Table 6 should only be taken as a qualitative marker for column size influence on separation, and not as absolute values.

Table 6: Calculated Resolution

Gradient Length (CV)	Resolution		
	6mL column	1mL column	0.5mL column
30	0.76	0.61	-
50	0.76	0.83	0.64
75	0.96	0.98	0.72
100	-	0.88	0.82
125	-	1.00	0.83

4.1.3.3 Peak Salt Concentration

For accurate determination of retention factors it is important to record the correct values for the peak salt concentration of each component. Otherwise, there is no linear correlation observed between the logarithms of normalized gradient slope and C_M and calculation of retention factors, according to the method outlined in Section 3.2.6 is not possible.

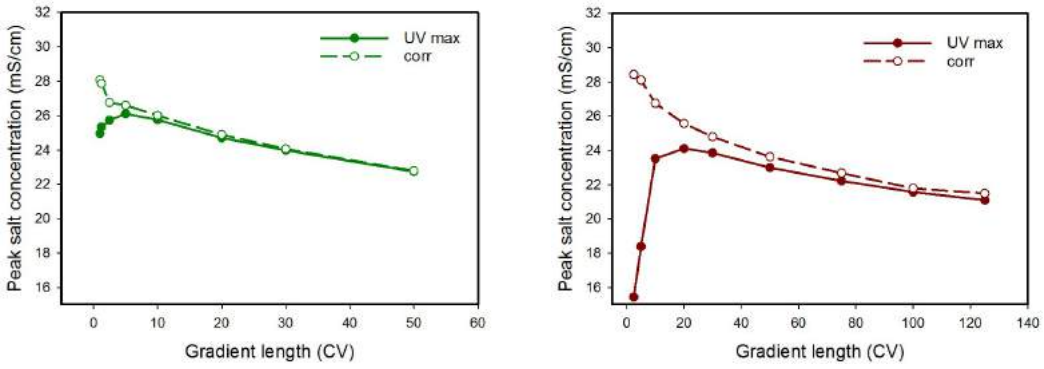

(a) 6 mL column

(b) 0.5 mL column

Figure 8: Influence of dead volume between UV and conductivity detector on peak salt concentration of BSA monomer

Figure 8 illustrates the need for factoring in the dead volume between UV and conductivity measurement cell in determining the exact peak salt concentration, especially for small column sizes and steep gradient slopes. The difference between recording the conductivity at the UV peak maximum and the corrected value is large, especially for small columns. The dead volume was determined to be $\sim$ 150µL using the method described in Section 3.

It was found, that peak salt concentration C_M is not constant between columns of different sizes. Increasingly small columns resulted in a decrease in peak salt concentration. To nullify the extra-column volume contribution a 40 mL Source 30 Q column was packed as a comparison. At longer gradient lengths the discrepancy is less pronounced as is shown in Fig. 9.

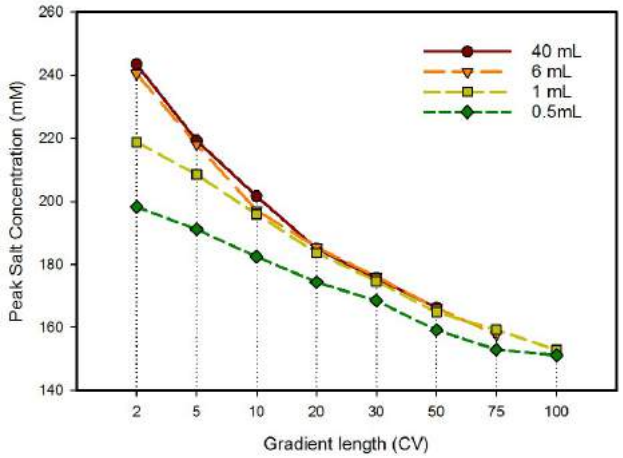

Figure 9: Influence of column size on corrected peak salt concentration of BSA monomer at specific gradient lengths

The only variable between these experiments was the column size. Recalling Eqs. (2.12) and (2.13), one can see that, as the phase ratio ϕ gets smaller, the peak salt concentration decreases.

$$C_M \sim [A(z+1)\gamma]^{\frac{1}{z+1}}$$

$$A = \phi K_e {q_0}^z$$

If an adjusted phase ratio ϕ_{app} is introduced to account for small column sizes the decrease in peak salt concentration can be correlated to an increased extra-column to column volume ratio. This is only valid for gradients of sufficient length, because of limitations imposed by the system. The total volume of short gradient lengths for small columns is not sufficient to nullify the system influence. The system volume is affecting the formation of the gradient, which results in the observed deviations in peak salt concentration. Deviations for long gradient lengths can not be explained this way. Here the proposed adjustment can help to illustrate the correlation between lower peak salt concentration and column size.

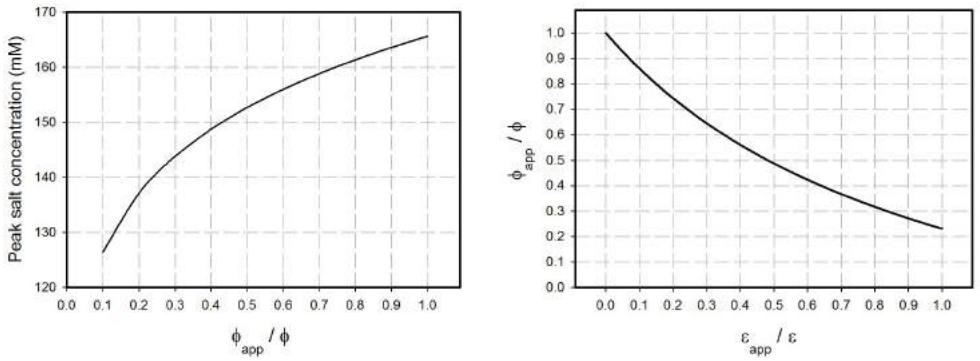

(a) Effect of lower ϕ on peak salt concentration 6 mL column

(b) Relation between void fraction increase and decrease in phase ratio

Figure 10: Correlation between extra-column volumes and peak salt concentration

Figure 10 shows, that a decrease in phase ratio leads to a lowered peak salt concentration. Using the pictured plots for larger column sizes, the increase in void fraction necessary to account for a lower C_M can be determined. The measured C_M value for the 0.5 mL column at γ 7 mM was $\sim$ 159 mM. The necessary phase ratio decrease is about 20% which equates to a void fraction increase of $\sim$ 18%. This is a feasible value for a 0.5 mL column constituting less than 100 µL.

Calculation for Fig. 10 was performed as follows for the 6 mL Source 30Q column, at a very shallow normalized gradient slope γ of 7 mM (equal to 50 CV). The column void fraction ε was determined to be 0.35, using the method outlined in Section 3.2.10. Values for z and A were taken from the monomer data in Table 10.

$$A_{adj} = \phi_{app} K_e {q_0}^z \quad \text{or} \quad A_{adj} = A\frac{\phi_{app}}{\phi}$$

$$C_M = [A_{adj}(z+1)\gamma]^{\frac{1}{z+1}}$$

The described influence is specific for small columns, because the contribution of extra-column volume decreases rapidly with increasing column size. Figure 9 shows little difference between the 6 mL and 40mL columns.

Bed volume determination is still based on measuring with a ruler. Reading errors increase with smaller column sizes, because the ratio of volume to bed volume is increasing. An incorrect bed volume results in wrong linearized gradient slopes, which are then not entirely comparable to LGE runs on other columns.

4.1.3.4 Determination of retention factors - Crude BSA

The determination of retention factors is a frequently used method for the characterization of proteins based on their charge properties at a given pH. It is desirable to perform most methods on small columns to limit the volume of consumed sample. If there is only a small quantity of sample available the use of small columns is unavoidable. However, accurate determination of retention factors using results obtained from small column is complicated by the increased influence of extra-column volumes.

Linear gradient experiments were carried out as described in Section 3.2.6 for all columns listed in Table 5 for crude BSA. The chromatograms of the LGE runs for crude BSA are shown in Fig. 6.

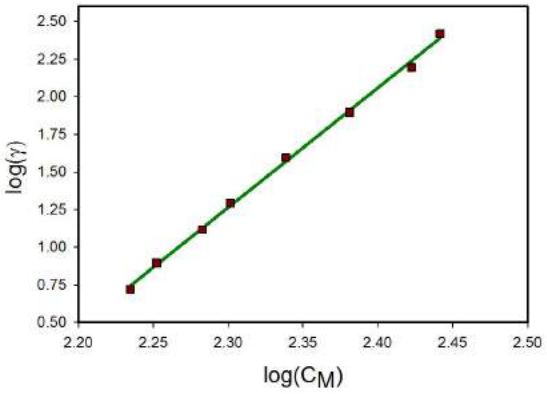

(a) 6 mL column

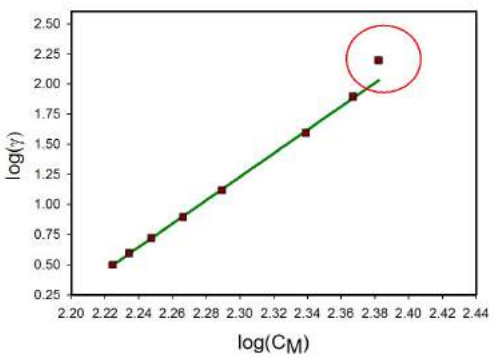

(b) 1 mL column

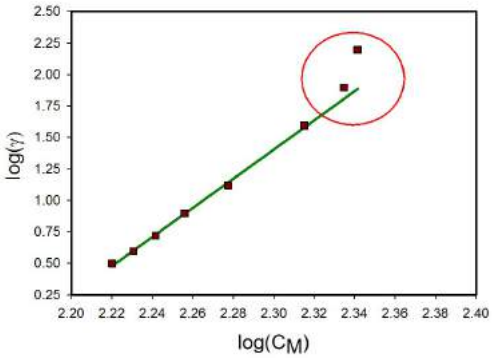

(c) 0.5 mL column

Figure 11: Plot of normalized gradient slope over recorded peak salt concentration - Crude BSA

Column size has an influence on the shape of the proposed linear correlation between the normalized gradient slope γ and the peak salt concentration C_M in Eq. (2.12). Figure

11 shows a side by side comparison of the log/log plots for crude BSA. The C_M values recorded at steep gradient slopes for small columns do not follow the model as discussed in Section 4.1.3.3. This is reflected in the clear increase in deviation from linearity of the data points highlighted in the red circle. These outliers were excluded from calculation and only the data points which show a linear correlation were used for calculation. Generally it can be said, that a decrease in column size correlates to a steeper slope in the log/log plots and thus to higher values for z and A as is indicated by the obtained values given in the table below.

Table 7: Crude BSA retention factors

Column Volume (mL)	**Retention factors** z	A
Monomer		
6	6.96	$1.39{\cdot}10^{16}$
1	8.73	$1.44{\cdot}10^{20}$
0.5	10.59	$1.56{\cdot}10^{24}$
Dimer		
6	11.01	$1.89{\cdot}10^{26}$
1	12.80	$3.13{\cdot}10^{30}$
0.5	10.79	$6.57{\cdot}10^{25}$

Table 7 shows all retention factors for the monomer and the dimer peak of the crude BSA sample runs. There are naturally fewer data points available for the dimer peak, because separation is only achieved at shallower gradient slopes. The peak salt concentrations for the dimer peak on the 6 mL column result in a straight line without outliers in the log/log plot similar to the plot in Fig. 11 .

4.2 Modelling

4.2.1 Preparation for modelling

As mentioned previously in Section 3.2.11, it was not possible at the time to accurately fit both the monomer and dimer peaks to one single experimental curve because of low resolution. Additionally peak-broadening caused by charge variants and multimers would also have distorted the parameter estimation of the film mass transfer coefficient and the pore diffusivity when fitting for just one component. Therefore it was decided to focus only on monomer runs. Fractionation was performed to separate pure monomeric BSA from a fraction containing largely dimer for subsequent experiments to determine physico-chemical properties of monomer and dimer.

4.2.2 Fractionation

Fractionation to obtain pure monomer and dimer for breakthrough curves and batch adsorption was performed using LGE in laboratory scale on a 40mL Source 30Q column and in pilot scale on a 630mL Source 30Q column. Sample load for both runs was 15mg protein per mL column volume. Gradient length was set to 30 CV and residence time was 3 min. Fractions for pure monomer and a sample with high dimer content were collected manually.

Laboratory scale

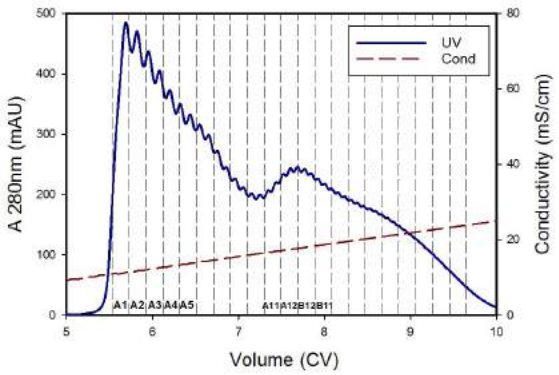

Figure 12: Fractionation on 40 mL Source 30 Q, sample load 15 mg/mL

Figure 12 shows the separation and the fractions pooled for batch adsorption experiments. SEC analysis of the sample pools was performed as outlined in Section 3.2.4
.

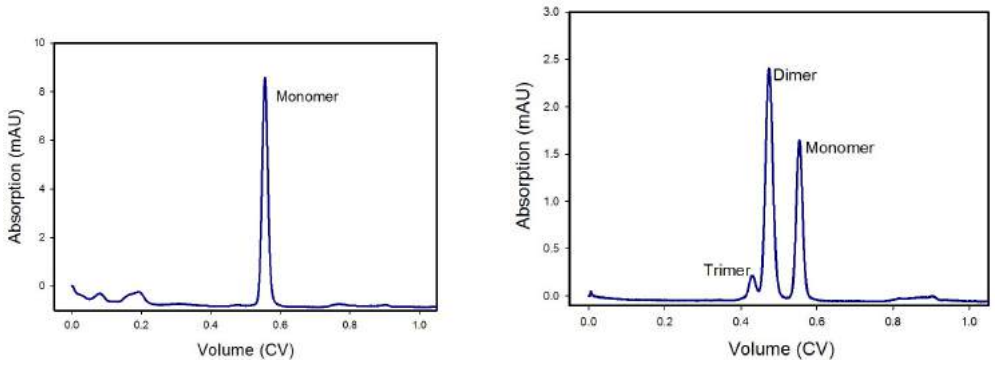

(a) Fractions A1-A5 (b) Fractions A11-B11

Figure 13: SEC Analysis of sample pools

Fraction A1 - A5 exhibited a high purity of BSA monomer with no other visible peaks. The peaks were fitted and integrated using PeakFit and show a multimer content of $\sim$ 60% in the pooled fractions A11-B11. These samples were used for batch adsorption experiments.

Pilot Scale

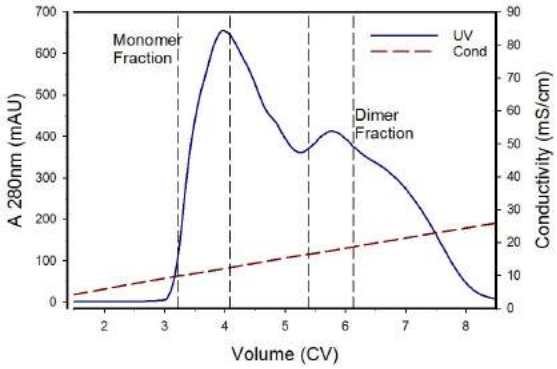

Figure 14: Fractionation on 630 mL Source 30 Q, sample load 15 mg/mL

Figure 14 shows the pilot scale fractionation run performed on a 630 mL column. Fractions were collected manually and SEC analysis was carried out.

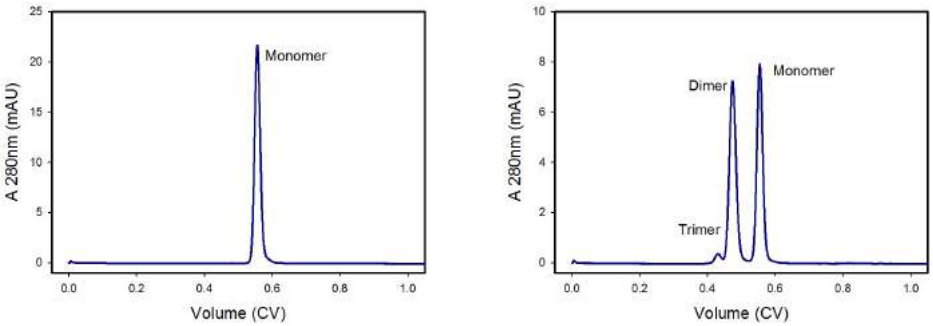

(a) Fractions A1-A5 (b) Fractions A11-B11

Figure 15: SEC Analysis of samples

Similar to the laboratory scale run the monomer fraction has a high purity with no visible multimer content. The multimer containing fraction was integrated using PeakFit and showed a multimer content of $\sim 50\%$. These samples were used for LGE experimental runs and in frontal analysis.

4.2.3 Determination of Isotherms

Batch adsorption experiments were performed on Source 30 Q resin with the original crude BSA sample, pure monomer and a mixture containing ∼60% multimer. Monomer and dimer samples were fractionated according to Section 4.2.2. The protein concentration of the samples was measured via UV-Vis spectroscopy. The resin was washed and 50% slurry was prepared using four different assay buffers. The final counter-ion concentrations in the assays were 16mM, 40mM, 64mM and 107mM Cl^- respectively.

Counter-ion concentration in the equilibration buffer was calculated using Henderson Hasselbalch Eq. (3.1):

$$7.5 = 8.1 + log_{10}(\frac{[A^-]}{[HA]})$$
$$-0.6 = log_{10}(\frac{[A^-]}{[HA]})$$
$$10^{(-0.6)} = \frac{[A^-]}{[HA]}$$

the concentration of the base is equal to the concentration of Tris $[A^-]$ in solution minus concentration of hydrochloric acid $[HA]$ added to the solution, which leads to

$$\frac{[A^-]}{[HA]} = \frac{([A^-] - [HA])}{[HA]}$$
$$10^{(-0.6)} = \frac{([A^-] - [HA])}{[HA]}$$
$$[HA] = \frac{[20mM]}{(10^{(-0.6)} + 1)} \longrightarrow \quad \sim \quad [Cl^-] = \quad \sim 16mM$$

Isotherms

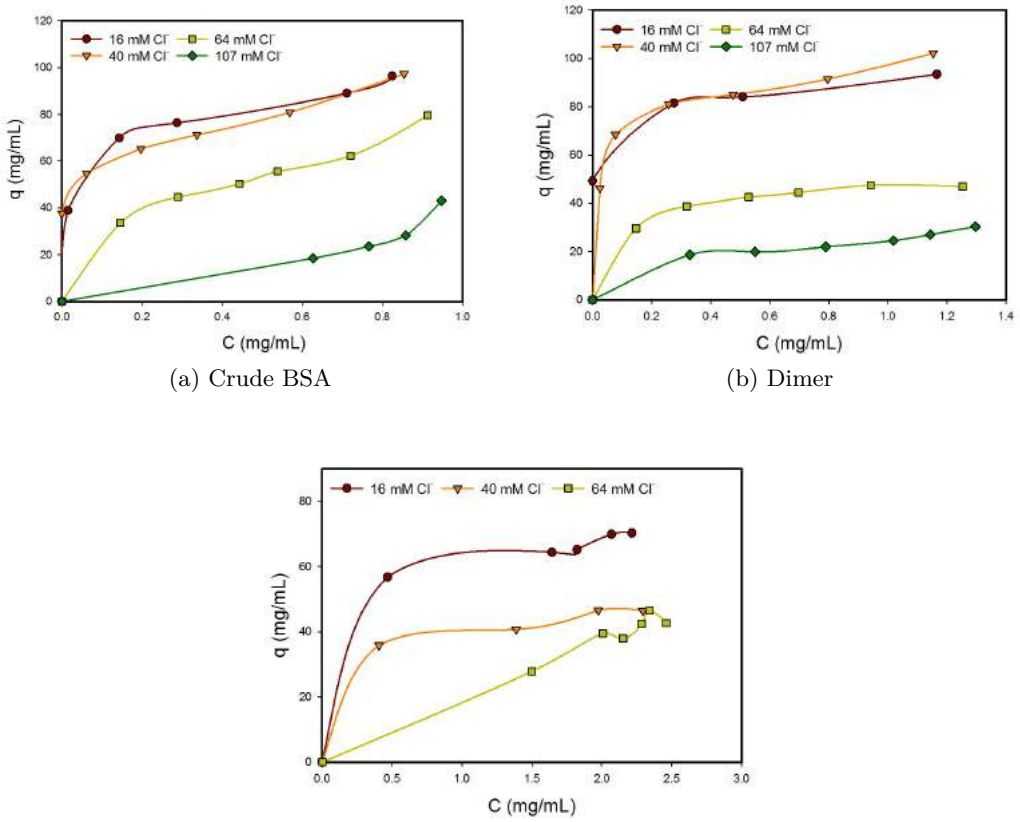

(a) Crude BSA

(b) Dimer

(c) Monomer

Figure 16: Adsorption Isotherms of Source 30Q for crude BSA, dimer sample and purified monomer at different counter-ion concentrations

The isotherms for crude BSA show that apparently no equilibrium state was reached after 24 hours. An error cause is the high multimer content, which influences the protein concentration measurement. Protein concentration is routinely measured and reported in mg/mL. The higher molecular weight of the aggregates causes a larger decrease of protein concentration in the supernatant when they are binding to the stationary phase. Displacement of the monomer during longer incubation times could also explain the isotherm shape. This is especially visible at high protein concentrations in the assay, where the particles could be saturated with aggregates if displacement reactions occur. This would lead to the effect observed in Fig. 16a, where the adsorbed phase concentration is increasing steadily. This conclusion is supported by the fact that the adsorbed phase concentration of BSA Monomer is already substantially decreased in the 40mM $[Cl^-]$ assays but the crude BSA and 60% Dimer assays remain unaffected by the in-

creased counter-ion concentration.

In the 60% dimer assay mixture (Fig. 16b) this effect is less pronounced, because of the higher dimer content. Although there is still no equilibrium state reached at high protein concetnrations. The non standard isotherm behaviour of the crude BSA sample without a clearly recognizable plateau interferes with the determination of SD or SMA model parameters for the BSA mixture.

Pure BSA Monomer (Fig. 16c) shows standard Langmuir isotherm behavior and a qm of **70mg/mL** under binding conditions. In light of the isotherm shapes of crude BSA it is important to consider the composition of any BSA sample used for determining qm of a chromatography resin by batch adsorption experiments. The same reasoning can be applied for other mixtures with high aggregate content.

SMA Model isotherm fit for BSA monomer

Figure 17 shows the result of a SMA parameter fit based on the batch adsorption data, where z, Ke and σ were fitted against the residual sum of squares of experimental isotherm data and the generated curves using the Excel solver. The total ionic capacity of the resin was fixed at 160 mM as determined by nitrate titration (see Section 3.2.10.

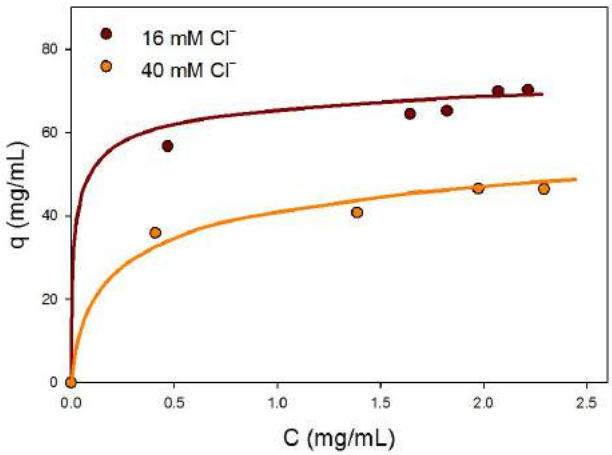

Figure 17: BSA Monomer isotherms at different counter-ion concentrations. Lines represent their respective SMA model fit

A comparison with the obtained z-values of BSA monomer listed in Table 7 shows that the value for z is lower in the SMA isotherm fit compared to the values obtained by LGE based determinatiion. The determination of retention factors is based on the stoichiometric displacement model and lumps all other parameters, e.g. K_e and q_0 into the parameter A, which is in itself highly dependent on the value of z. In the SMA model isotherm fit above, the total ionic capacity was fixed and the inclusion of the shielding coefficient in the equation results in lower z values than in the SD model. Due to the

different nature of both model fits, they are not interchangeable. Recalling Eq. (2.13) for the lumped parameter A the K_e at a q_0 of 160 mM can be calculated. The value is in good agreement with the value obtained by the SMA model fit. However, using the parameters determined by LGE experiments and setting the shielding coefficient σ to zero, effectively converting the SMA isotherm to the SD isotherm, the isotherm could not be fitted, which suggests, that the model parameters obtained by one method may not be interchangeable with parameters obtained from another method.

Table 8: SMA model Parameters - Isotherm fit

Parameter	SMA Isotherm fit	Published data [18]
z	3.8	3.7
σ	118	171
q_0	160 mM	883 mM
K_e	2.56	0.081

Comparing the model parameters in Table 8 above with data for BSA at a pH of 7, published by Susanto et al. [18] shows a large difference in the equilibrium constant and in the shielding coefficient. The main difference lies in the total ionic capacity and the shielding coefficient. The published data reports a total ionic capacity of 883 mM for the Source 30Q resin, which is well outside of the range of reported values for ion-exchange resins. It must be noted however, that adsorption equilibrium models can often not be applied when too constrained by physical parameters. If one parameter is excluded from fitting then another parameter has to compensate for the loss of the degree of freedom in fitting. The implications of this limitation of the model and general applicability are discussed in Section 5.

4.2.4 Determination of pore diffusivity D_e

The pore diffusion coefficient D_e for BSA was determined by frontal analysis according to the method in Section 3.2.9 and by pulse experiments under non-binding conditions as described in Section 3.2.8.

4.2.4.1 Frontal analysis

Breakthrough curves were generated on a 6 mL Source 30Q column for original Bovine Serum Albumin (BSA) sample, pure monomer and 50% dimer sample. The samples were produced by fractionation in pilot scale (Section 4.2.2) . All samples were loaded onto the column in 20mM Tris/HCl pH 7.5 running buffer. The curves were normalized against the bypass absorption of the applied sample.

Crude BSA

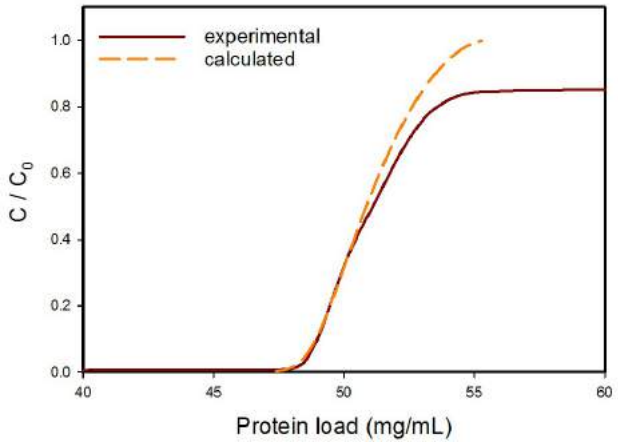

Figure 18: Frontal Analysis - Crude BSA sample

Figure 18 shows the curve fit using the shrinking core model constant pattern solution mentioned in Section 3.2.9 for curve fitting and parameter estimation. The crude BSA sample contains $\sim$ 20% multimers. It exhibits long tailing over a long sample loading caused by displacement of the monomer by the dimer. Calculated q_m was $\sim$ 77 mg/mL.

Pure monomer

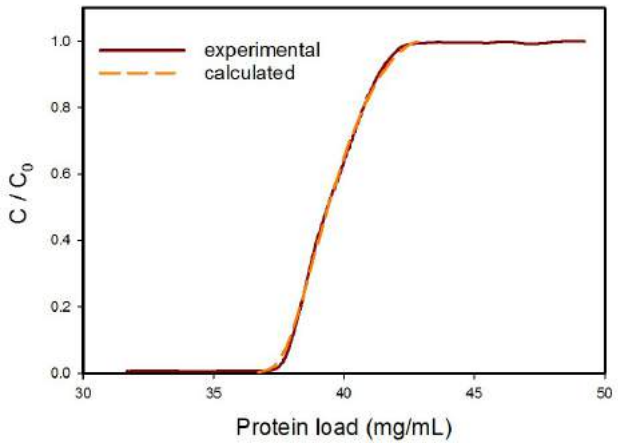

Figure 19: Frontal Analysis - Crude BSA sample

In contrast to crude BSA, the pure monomeric BSA shows a sharp profile and equilibrium was rapidly achieved. The calculated maximum binding capacity q_m of 60 mg/mL was also in good agreement with the results from isotherm experiment in Section 4.2.3 .

Dimer fraction

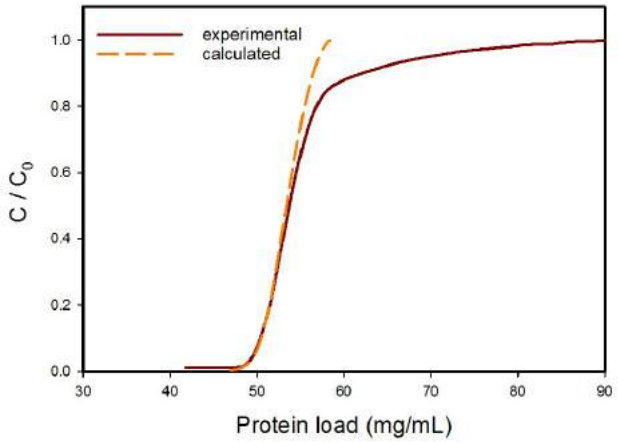

Figure 20: Frontal Analysis - 50% Dimer sample

The sample containing $\sim$ 50% dimer exhibits a faster displacement reaction and reaching of equilibrium than the crude BSA sample. The calculated q_m was 81 mg/mL.

Table 9: Frontal analysis - Parameter estimation

Sample	k_f (cm/sec)	D_e (cm^2/sec)	q_m (mg/mL)
Crude BSA	$6{\cdot}10^{-4}$	$4{\cdot}10^{-8}$	**77**
Monomer			**60**
50% Dimer	$2.5{\cdot}10^{-4}$		**81**

The observed tailing in the frontal analyses are in agrrement with published results by Hunter and Carta [37]. The effective pore diffusivity of BSA was low at $\mathbf{4{\cdot}10^{-8}\ cm^2/sec}$ for all samples. This may be an indication of some hindrance to pore diffusion. The paper published by Susanto et al. [18] suggested the implementation of a hindrance parameter to estimate the effective pore diffusivity at different concentrations of adsorbed BSA on the stationary phase. Performing the calculation as outlined in this publication the fastest pore diffusion of BSA is $\mathbf{3.8\ {\cdot}10^{-7}\ cm^2/sec}$ at $q = 0$.

4.2.4.2 Pulse experiments

D_e obtained by frontal analysis was very low, compared to the free diffusivity of BSA, which is $\sim 6{\cdot}10^{-7}$ cm^2/sec. To investigate the pore diffusion without any interaction with the stationary phase effective pore diffusion was estimated for BSA under non-binding conditions as outlined in Section 3.2.8. Figure 21 shows a plot of the van Deemter analysis results including the linear regression.

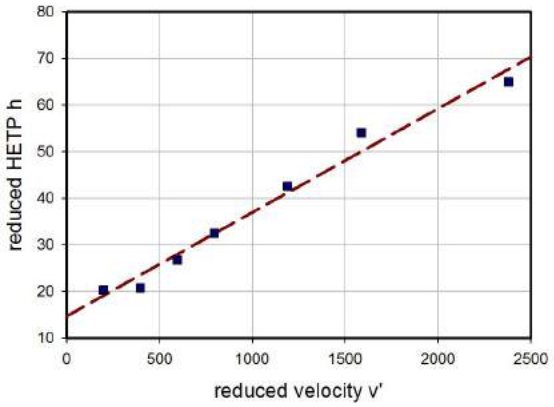

Figure 21: Plot of van Deemter Analysis - crude BSA

D_e was calculated to be $\sim$ **1 $\cdot 10^{-7}$ cm^2/sec** depending on the Sherwood number at the given operating conditions. This is more than twice as fast as the value determined by frontal analysis above.

4.2.5 Determination of retention factors - Fractions

For the determination of the retention factors of the monomer, a 40 mL column was packed to ensure, that the extra-column influence could be excluded as a cause for underestimating the peak salt concentration and to compare the values obtained from a large column to those of smaller columns.

4.2.5.1 Purified BSA Monomer

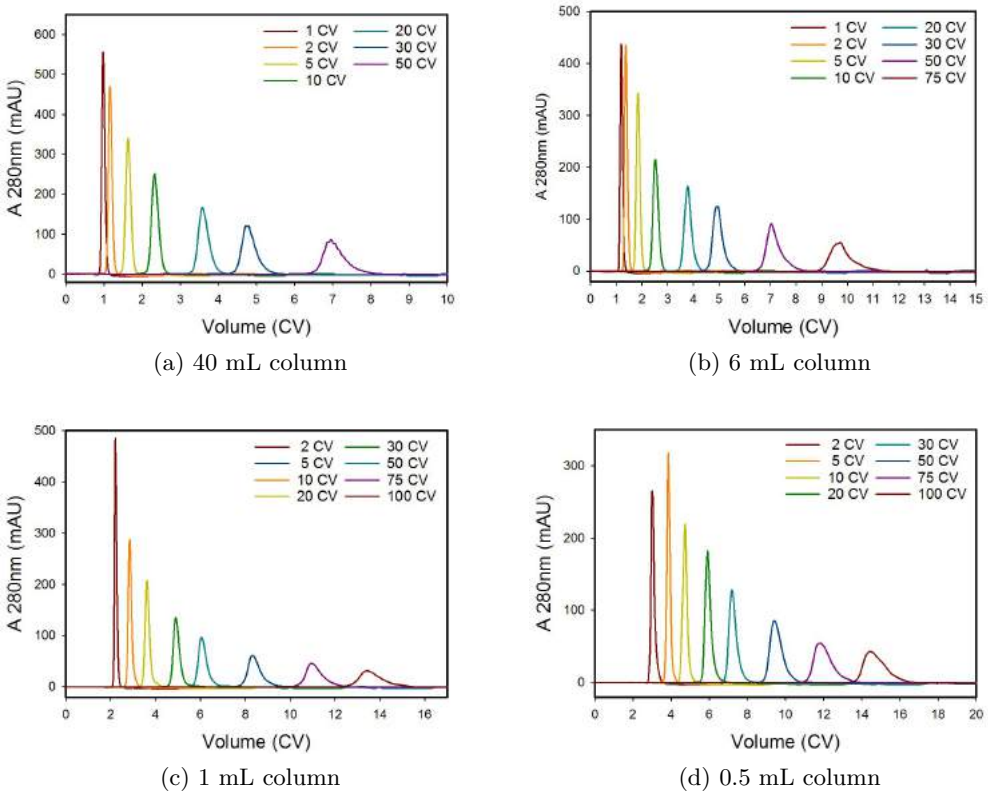

(a) 40 mL column

(b) 6 mL column

(c) 1 mL column

(d) 0.5 mL column

Figure 22: LGE experiments performed with BSA monomer on different columns with increasing gradient lengths

Table 10 shows the results obtained from the LGE experiments carried out on the laboratory scale Source 30Q columns listed in Table 4.

These values suggest that a 6 mL column is sufficient to obtain accurate results, since the retention factors are highly similar to those calculated from experiments performed on a 40 mL column. Again, as observed when using crude BSA, a decrease in column size leads to a non-linear relation in a log/log plot and an increase in z and A.

Table 10: BSA Monomer retention factors

Column Volume (mL)	**Retention factors** z	A
40	7.51	$1.35 \cdot 10^{17}$
6	7.52	$1.38 \cdot 10^{17}$
1	8.61	$3.11 \cdot 10^{19}$
0.5	10.42	$1.80 \cdot 10^{23}$

4.2.5.2 60% Dimer sample

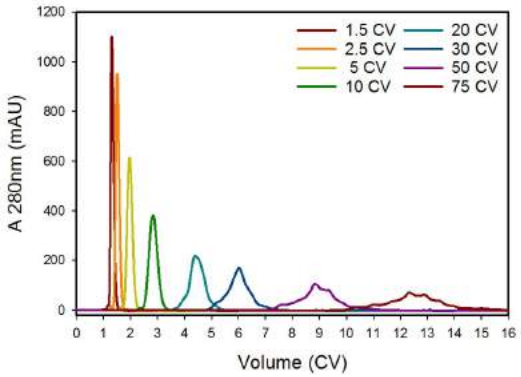

Figure 23: LGE of dimer sample on 6 mL column with increasing gradient lengths

Figure 23 shows, that no visible separation of variants occurs when performing LGE for any gradient lengths even while loading in the linear range of the isotherm. This was corroborated by an analytical run on a 1mL Mono Q column with a very shallow gradient (data not shown). Therefore, no determination of retention factors for the BSA dimer was possible using the sample with 50% multimer content.

4.2.6 Modelling of System - ÄKTA Explorer

As described in Section 2.6, a chromatography system can be modeled as PFR and series of single CSTRs. This was realized for the ÄKTA Pilot and ÄKTA Explorer 100 system using step input of elution buffer 1 M NaCl.

The built-in buffer mixer of the ÄKTA Explorer system has a volume of 0.6 mL. Parameter estimation of a CSTR showed, that the effect of the real mixer is equal to a CSTR of the same volume. The tubings with a diameter of 0.75 mm were measured where possible and the rest of the delay volume was fitted using CadetMatch to obtain

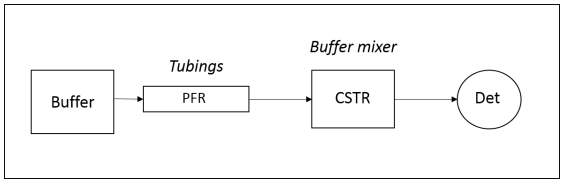

Figure 24: ÄKTA Explorer 100 system model

the length of the PFR for each application. Axial dispersion was neglected for the fit of the salt transition.

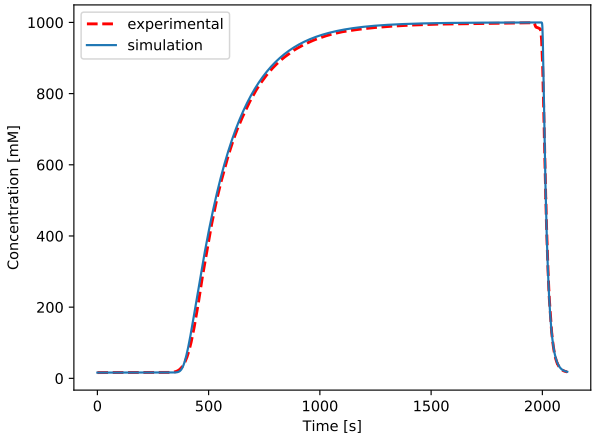

Figure 25: ÄKTA Explorer - Bypass fit example for flowrate 0.2 mL/min

Table 11: Äkta Explorer System volumes

PFR length (m)	CSTR (mL)
2.8	0.6

It has to be noted that the PFR length presented here is just applicable to this parameter estimation. The length has to be adjusted for every new column and position because of variable tubing length and column system type, this explains the higher variability in length of the PFR during modeling. The system pumps also influence the delay volume because of inherent ramp up and slowing down to reach the programmed flow rate, the volume/time ratio differs from the programmed conditions in the model, where the flow rate changes are instantaneous. The important part of the curve is the shape of the salt transition which is only influenced by the CSTR.

4.2.7 Chromatographic Modelling

After determination of the retention factors for the SD model, the next step was using CadetMatch and experimental runs to determine the SMA model parameters for BSA monomer and dimer. As mentioned previously in Section 4.2.1, it was not possible at the time to accurately fit both the monomer and dimer peaks because of low resolution. The peak broadening caused by possible charge variants would also have distorted the parameter estimation of the film mass transfer coefficient and the pore diffusivity when fitting for just one component. Therefore it was decided to focus only on monomer runs. The total ionic capacity of the resin was determined by $NaNO_3$ pulse experiments, described in Section 3.2.10. Effective pore diffusion was estimated under non-binding conditions as outlined in Section 3.2.8.

Table 12: Experimentally determined parameters

Parameter	Value	Unit
Void fraction ε	0.35	-
Particle porosity ε_p	0.53	-
Total ionic capacity q_0	160	mM
Pore diffusivity D_e	$\sim 1{\cdot}10^{-7}$	cm^2/sec

Table 12 shows all experimentally determined parameters for both the column and BSA sample obtained by the methods outlined in Section 3.2. The effective pore diffusivity of BSA measured under non-binding conditions is faster than the value obtained by frontal analysis. The parameters listed above were used to generate a simulation file which formed the basis for the fitting process. Other parameters were set to values which nullify their contribution to peak shape and position to reduce computation time and make interpretation easier. For example axial dispersion in the column was set to a very low value where the impact of dispersion caused by the column was essentially zero, so all peak broadening effects were lumped into the fitted parameters.

The monomer LGE run used for fitting was performed on a 6 mL column at a gradient length of 10 CV. This gradient length was chosen after examining the LGE runs performed for the determination of the retention factors, because there was no observed irregular peak broadening caused by a possible charge variant contained in the monomer sample.

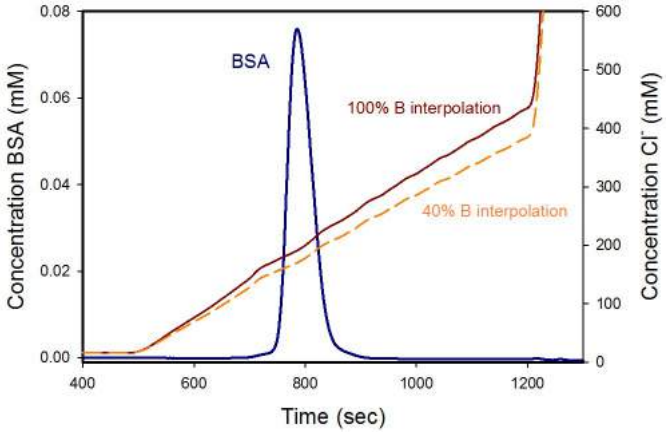

Figure 26: Monomer LGE run with gradient length of 10CV - different interpolation methods for salt gradient are shown

As previously discussed in Section 3.2.11 the conversion for the salt gradient is done by interpolation. Typically the endpoint chosen is the conductivity at 100% elution buffer. The correlation between conductivity and ion concentration is not linear at high concentrations. After conversion the observed slope of the salt gradient is steeper than the theoretical slope by $\sim 11\%$, resulting in a higher apparent peak salt concentration which is not congruent with actual counter-ion concentration. Figure 26 shows the discrepancy between the two interpolation methods. The gradient end was programmed for 40% B which corresponds to ~ 41 mS/cm. Interpolating between conductivity values for 0 - 100% elution buffer results in a gradient end higher than the calculated value of 416 mM Cl^-. Interpolating to 40% B mitigates the effect and the endpoint is much closer to the calculated value and the slope is nearly identical to the theoretical slope.

The theoretical gradient slope is calculated as follows

$$\text{slope} = \frac{[Cl^-]_{end} - [Cl^-]_{start}}{t_G}$$

Different optimizations were performed to identify the effect of this conversion error on the SMA model parameters.

The previously established ÄKTA Explorer system model was used as a basis for this fitting process. The PFR length was adjusted manually to match the salt transitions.

4.2.7.1 Parameter Fit 1

The first parameter optimization run was performed with the first interpolation method normalized to the conductivity of the elution buffer. The discrepancy between the interpolated and theoretical gradient slope was noticeable. The experimental slope was fitted using linear regression with TableCurve2D.

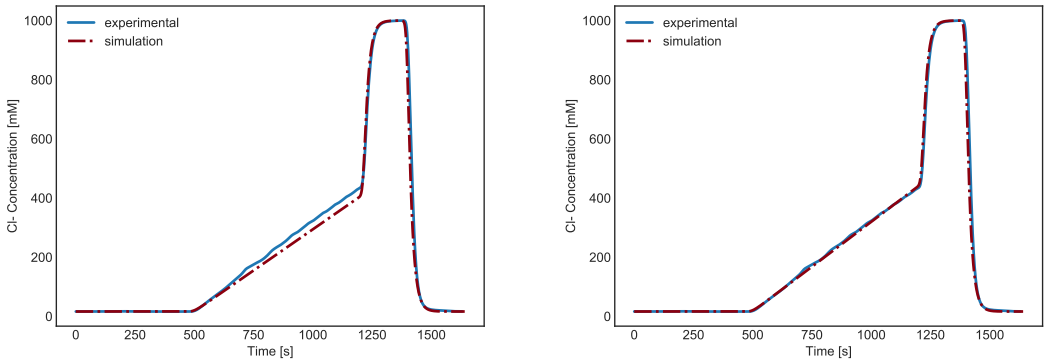

(a) Salt gradient - theoretical slope

(b) Salt gradient - experimental slope

Figure 27: Comparison between theoretical and experimental slope for interpolation method to 100% B

Figure 27 shows the discrepancy between the theoretical slope and the fitted experimental slope after conversion. The Cadet inlet unit operation is programmed by setting the salt concentration in the equilibration buffer as a constant and a slope in mM/sec in a linear equation to generate a linear gradient over the gradient length.

After fitting the salt gradient, the parameter optimization was performed for the SMA model parameters z, σ and K_e. To incorporate the peak shape into the fitting process the effective pore diffusivity D_e was also set as an optimization parameter.

4.2.7.2 Parameter Fit 2

The second parameter optimization procedure was performed analogous to Fit 1, the sole difference being the conversion of the salt gradient. The modified interpolation method shows a better fit for the calculated theoretical slope.

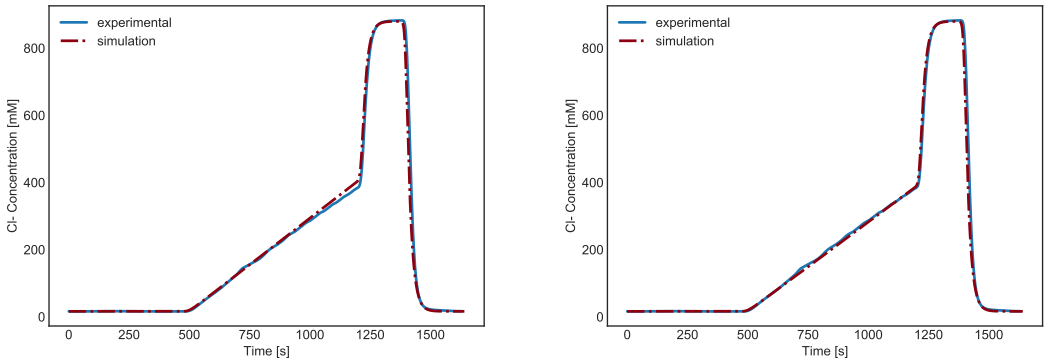

(a) Salt gradient - theoretical slope

(b) Salt gradient - experimental slope

Figure 28: Comparison between theoretical and experimental slope for interpolation method to 40%B

The adjustment only works in lower molar ranges, as can be seen in Fig. 28, because of the non-linear relationship between conductivity and concentration [36], an increase in accuracy in the lower molar range leads to a decrease in accuracy in higher molar ranges. The concentration of the 1 M NaCl step input is reduced by a factor of $\sim$ 11 % which is exactly the difference of the slopes of the different interpolation methods. In most applications this is not crucial and accuracy in lower molarity regions is more desirable. It should be noted, that the difference is immaterial when converting the peak salt concentration back to mS/cm by the same method. These differences are only important when an accurate estimation of the counter-ion concentration is crucial, for example when simulating a step elution. SMA parameters are affected and will be different because of the different peak salt concentrations.

Table 13: Values obtained by parameter optimization with 6 mL column

Parameter	Fit 1	Fit 2	Unit
z	6	5	-
σ	94	85	-
K_e	4.56	2.20	-
D_e	$1.56{\cdot}10^{-7}$	$1.99{\cdot}10^{-7}$	cm^2/sec

Table 13 shows the obtained parameter from both fitting procedures compared to the experimental results. As expected, the parameters of Fit 1 show a higher effective charge, more shielding and a higher equilibrium constant than Fit 2, which is directly correlated to the higher peak salt concentration represented in the chromatogram.

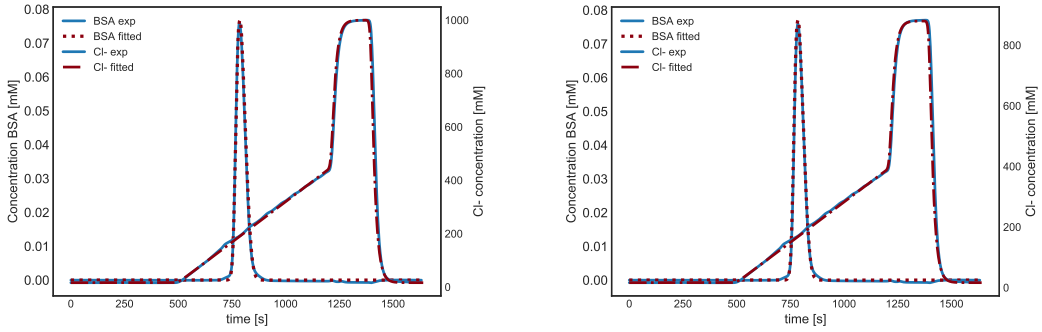

(a) Result Fit 1

(b) Result Fit 2

Figure 29: Parameter optimization results - Experimental curves compared with the simulated chromatogram of a 6 mL column using the parameters obtained by both fits

The PFR length was adjusted manually. The inner tubings of the workstation had to be replaced, thus the PFR length at 2.25 m was actually smaller than the bypass length. The inner tubings of the systems had to be replacedrepresent the rest of the dead volume of the system without the CSTR contribution 2.65 Due to the discrepancies between the tubings and column systems this has to be done for every column separately. CadetMatch generates numerous results during the fitting process, some with very close match scores. A challenge in multi-objective parameter estimation is the decision which parameter set is able to accurately simulate chromatographic runs with new input parameters, such as flow rate or sample loading. If the system has too many degrees of freedom, the results can be very diverse, resulting in too many parameter sets with the same matching score but different values for the parameters. On the other hand, if too few variables are set as fitting parameters, it may be impossible to generate an acceptable result. For these parameter optimizations it was decided to use discrete values for z and σ to decrease the degrees of freedom for the fitting algorithm. If more than three parameters are fitted at the same time, it is not possible to visually evaluate the set of possible parameters, depending on the correlation between the parameters, because of the necessity to include the match score as an axis to evaluate the fit, four-dimensional space would be reached with more than two parameters. To visualize the parameter fit for BSA Monomer, three parameters z, D_e and K_e were used to generate a 3D scatter plot. A colormap was used to represent the match score of the parameter sets to evaluate the fit performance and visualize a solution space.

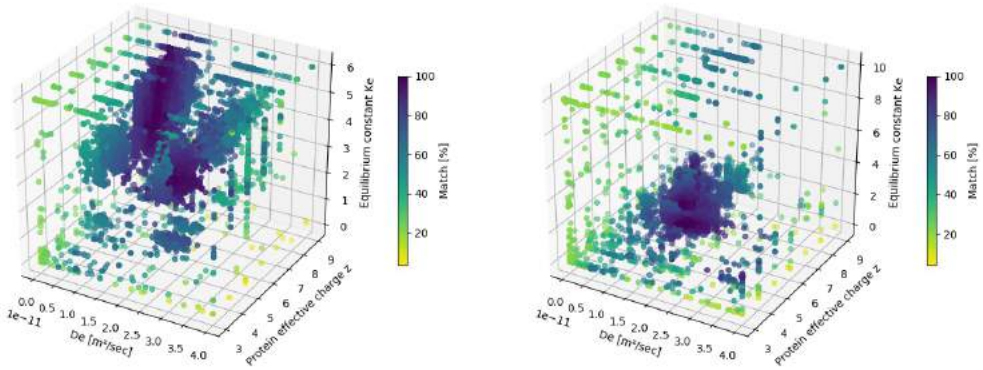

(a) Fit 1 (b) Fit 2

Figure 30: Illustration of solution space

Figure 30 illustrates the difficulty in evaluating the parameter optimizations visually. The only difference between the two fits was the salt gradient, yet the solution space is drastically different. The true solution space for the parameter estimation fit performed is hyper-dimensional. The values listed in Table 13 are results with the highest match score for each fit, which, depending on the scoring algorithm, is the best way to choose a parameter set. The most logical way to verify the obtained SMA model values is to perform forward simulations and compare the results to experimental runs. It has to be noted that, when simulating a column, the difference in packing quality may impact the peak shape, especially in smaller columns. The evaluation of the parameter fit is therefore based on the obtained peak salt concentration. There are a number of parameters which can be adjusted to incorporate the packing quality into the column model itself, e.g. column dispersion.

4.2.7.3 Evaluation of parameters with isotherm data

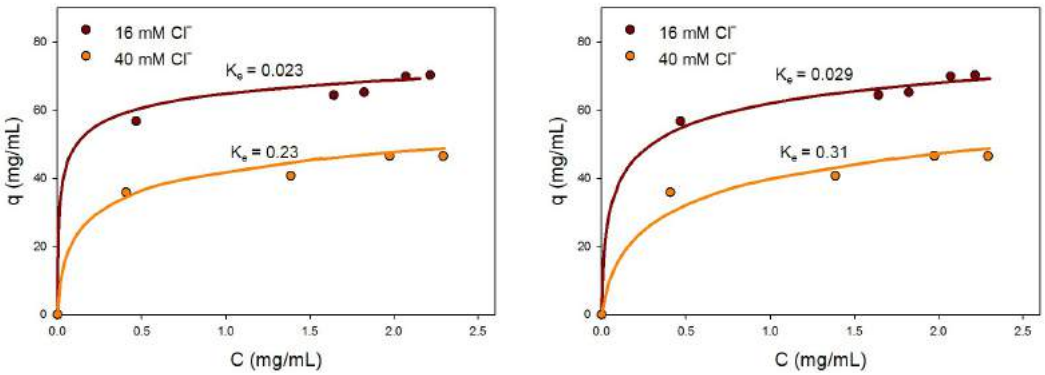

(a) SMA isotherm with Fit 1 parameters

(b) SMA isotherm with Fit 2 parameters

Figure 31: SMA isotherms for BSA monomer calculated using parameters in Table 14. shown with experimental data points

Utilizing the parameters from Table 13 to fit the monomer batch adsorption data with the SMA model revealed that they cannot be directly used for fitting the data. The parameters were entered into Excel and a curve simulation was generated and compared to the experimental curve. The equilibrium constant was adjusted for both parameter sets to fit the curves. It was necessary to increase the K_e value for the assay with higher counter-ion concentration. The shape of the isotherm demonstrates the differences between the two fits. Fit 1 showed a higher z value which correlates with a more rectangular shape. The equilibrium constants of the two fits are very similar for their respective counter-ion concentration.

Table 14: SMA isotherm parameter comparison - CadetMatch parameter sets compared to isotherm fitting see Section 4.2.3

Parameter		Fit 1	Fit 2	SMA isotherm fit	Published data [18]
z		6	5	3.8	3.7
σ		94	85	118	171
q_0			160 mM		883 mM
K_e	16 mM	0.023	0.029	2.56	0.081
	40 mM	0.23	0.32		

Table 14 shows a comparison of all parameters used in fitting SMA model isotherms. The values for the SMA model parameters obtained by performing the fitting procedure

using a chromatographic run in CadetMatch and the outcome of isotherm data fitting are not in line with each other, most likely due to the fundamentally different nature of the methods. The applicability of the SMA model and the fitting procedure differences is discussed further in Section 5.

4.2.7.4 Prediction of peak salt concentration

LGE simulations were performed with theoretical gradient slopes to compare them to the experimental runs performed on 40 mL, 6 mL and 0.5 mL columns for the BSA monomer. The simulations were done for both fits and interpolation methods. Fit 1 values were compared to the experimental peak salt concentration calculated by interpolation normalized to the conductivity at 100% B and Fit 2 values with interpolation between 0 and 40% B.

Additional columns were simulated to represent the physical 0.5 and 40 mL columns. The 6 mL column model was identical to the model used for parameter optimization. The values listed in Table 12 were used for all columns. The D_e was adjusted based on the values obtained from both parameter optimizations.

The obtained chromatograms were fitted with peak fit and the peak salt concentration at the first moment (rounded) was taken for comparison.

Table 15: Calculated peak salt concentration C_M for forward prediction on different columns and deviation from experimental peak salt concentration of BSA monomer runs Section 4.2.5

Gradient length (CV)		C_M (mM)		C_M exp. (mM)		Deviation (%)	
		Fit 1	Fit 2	norm 100%	norm 40%	Fit 1	Fit 2
40 mL column	5	223	204	219	198	1.7	3.2
	10	200	182	202	182	0.8	0.1
	20	181	161	185	167	2.1	3.6
	30	171	151	176	159	2.6	4.8
6 mL column	5	214	196	218	196	1.7	0.2
	10	195	173	197	178	0.8	2.4
	20	174	154	185	167	5.9	7.7
	30	163	144	176	159	7.1	9.4
0.5 mL column	5	215	194	191	172	12.6	12.8
	10	197	177	182	165	8.1	7.7
	20	180	159	174	157	3.3	1.0
	30	170	150	168	152	1.0	1.4

Table 15 shows the difference between the interpolation methods clearly. The counter-ion peak salt concentration of Fit 2 is lower by $\sim$ 20 mM for all columns and gradient lengths. The deviation between simulated and experimental results is lowest for the 40 mL column model. Interestingly the trend in deviation is not the same at all column sizes. The deviation increases for the larger columns but decreases in the 0.5 mL column with gradient length. The reason for this behavior is still unclear, but it is likely caused by different peak shapes or the influence of the extra-column volume on the experimental peak salt concentration values of the small column. It is important to consider, that with increasing gradient length a given deviation in peak salt concentration results in progressively worse retention time prediction, because of shallower slopes. For example, a deviation of 10% at a gradient length of 30 CV with a gradient slope of 0.185 mM/sec is equivalent to a deviation of $\sim$ 75 seconds or 0.4 column volumes.

Table 15 was generated by fitting only one LGE experiment on one column. To improve the parameter optimization multiple options may be explored. The fitting procedure could be performed for multiple columns and gradient lengths. The effective protein charge could be fitted as a rational number instead of an integer, since it has the largest impact on the model this could help to refine the parameters. The total ionic capacity could also be included as a fitting variable. Additionally film mass transfer and column dispersion could be fitted to reduce the influence of a change in the SMA model parameters on peak shape. However, all these changes increase the computation time and difficulty in choosing a working parameter set.

4.3 Scale-up

Scale up predictions and experiments in this work were performed by establishing a system model for the ÄKTA Pilot system and investigating the mixing behavior of the built-in bubble-trap to characterize the extra-column effects. Later a 630 mL Source 30 Q column was packed to investigate separation of BSA monomer and dimer in the pilot scale. Prediction of elution profiles at higher sample loads was performed to investigate the change in retention time.

4.3.1 Comparison of BSA Separation - Scale up to Pilot scale

A Fineline 100 column system from GE Healthcare was packed to a column volume of 630 mL with Source 30 Q resin on an ÄKTA Pilot system to characterise the BSA separation in pilot scale.

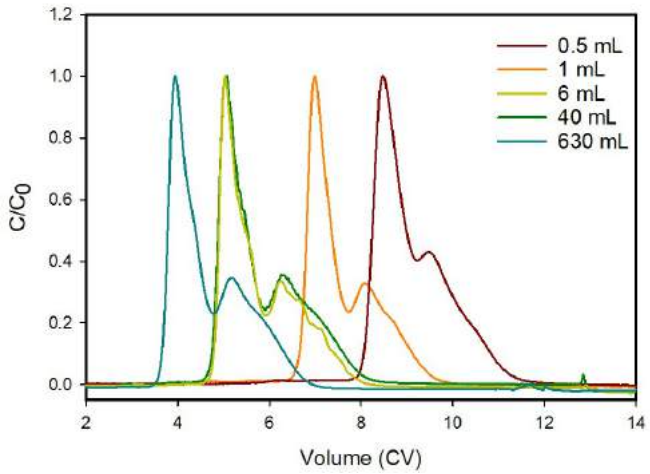

Figure 32: Crude BSA separation on columns of different size, gradient length 30 CV

Figure 32 shows the separation of crude BSA for all columns packed for this work at a gradient length of 30 CV. At the beginning only the smaller scale columns were available, the 630 mL and 40 mL columns were packed after the preliminary testing and determination of the retention factors of crude BSA. The separation was found to be highly uniform across all column sizes. A difference in resolution between the 630 mL, 40 ml and 6 mL column is not visible when exclusively looking at the chromatogram. However, on the 0.5 mL column the peak width is visibly larger and the dimer peak is only slightly separated. The increased width of the peaks at shallower gradients contributes to the decrease in resolution that is observed in Table 16. This peak broadening could be caused by extra-column effects or by increased separation of charge variants of the sample.

The relative resolution and shape of the curves suggest, that a scale up to 630 mL can be performed with model parameters obtained from a 6 mL column. Results from the determination of retention factors have shown that parameters for the BSA monomer obtained from LGE experiments on the 6 mL column are identical to parameters from the 40 mL column (Section 4.2.5). The different retention volumes show the relative nature of normalizing volume with the column volume. A larger difference between the system volume and the column volume leads to a longer retention time in CV at the same gradient length. This also is an indicator as to the contribution of extra-column effects to the separation. The delay volume of the curves for 6 and 40 mL column is practically identical, which also implies that the differences between these columns in extra-column effects are negligible. The delay volume is even less for the ÄKTA Pilot System and the Fineline 100 column, which is indicative of a favourable system to column volume ratio.

Table 16: Comparison of Resolution between BSA Monomer and Dimer peak

Gradient Length (CV)	**Resolution**			
	630mL column	6mL column	1mL column	0.5mL column
30	0.74	0.76	0.61	-
50	-	0.76	0.83	0.64
75	-	0.96	0.98	0.72
100	-	-	0.88	0.82
125	-	-	1.00	0.83

4.3.2 Influence of bubble-trap on BSA Separation

The ÄKTA Pilot system has a built in bubble-trap to protect air from entering the column. Preliminary salt transition experiments showed, that the mixing behaviour inside the bubble-trap does not influence the slope of a linear gradient. However, there was a noticeable difference in the variance of a step input when comparing the system bypass to the bubbletrap. Experiments were carried out for crude BSA samples at analytical loads to determine whether there is an influence on separation or not. A 630 mL Source 30Q column was loaded with 1.5 mg/mL crude BSA solution. LGE was performed at a gradient length of 30 CV with and without connecting the bubble-trap. Additionally step elution was performed at 20%B, with and without the bubble-trap.

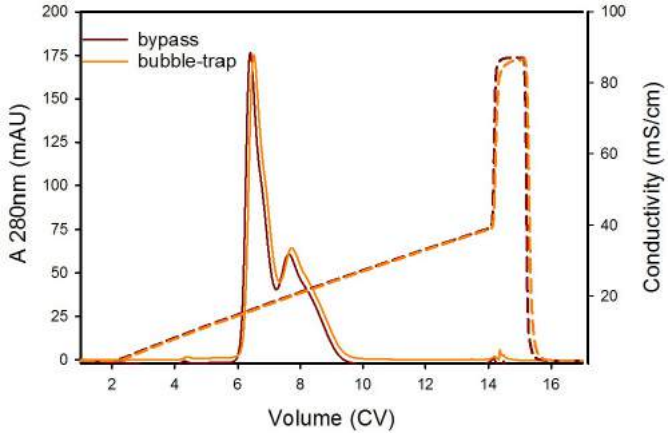

Figure 33: LGE with gradient length of 30CV, sample load 1.5mg/mL

Figure 33 shows that LGE is not impacted by the addition of the ÄKTA Pilot bubble-trap. The gradient slopes are identical and only the delay volume is increased by the volume of the bubble-trap. The only discernible influence is seen during the clean step, where the salt step transition takes longer.

There is, however, a clear influence on the peak width when performing a step-elution as evidenced by the run shown in Fig. 34. Performing an EMG fit of the peaks with PeakFit revealed a $\sim$ 20% increase in peak width at the base and an 80 % increase in variance. Since all process parameters were kept constant the increase in peak width can be wholly attributed to the bubble-trap and connecting tubes. Examination of the salt transition curve shows a large residence time difference between the bypass and the bubble-trap.

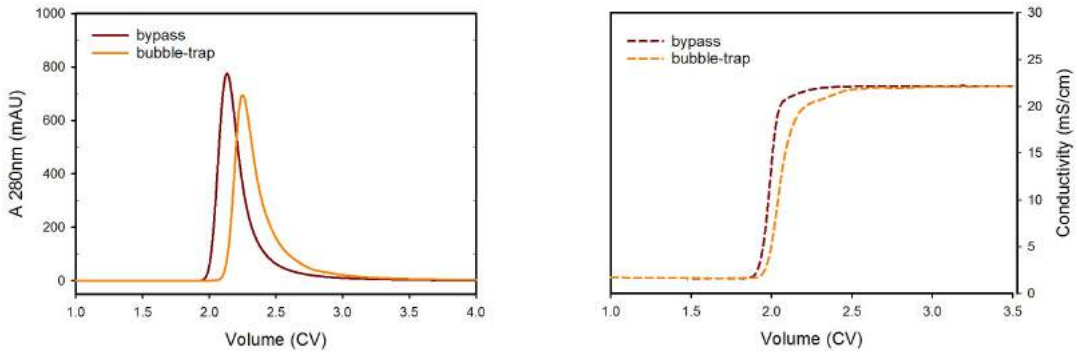

(a) Peak width comparison

(b) Salt transition

Figure 34: Step Elution Experiment 20% B, sample load 1.5 mg/mL

The irregular mixing behavior observed during step elution was the basis for the following experiments to determine the exact nature of the flow behaviour inside the bubble-trap.

4.3.3 Modelling of system - ÄKTA Pilot

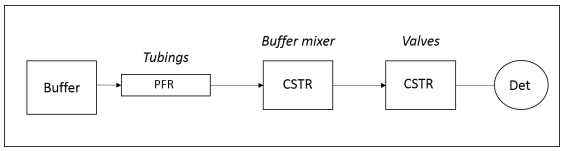

Figure 35: ÄKTA Pilot system model

Figure 35 shows the chosen model for the ÄKTA Pilot system. The buffer mixer of the ÄKTA Pilot System has a volume of 5mL which was modeled as a CSTR. The tubings were modeled as a PFR with an internal diameter of 2.9 mm. All Valves and dead volumes of the system were lumped together into a single CSTR. A fit was performed with CadetMatch to obtain values for the second CSTR and the total length of the PFR. The shown graphs for fitting are plotted and saved automatically by CadetMatch.

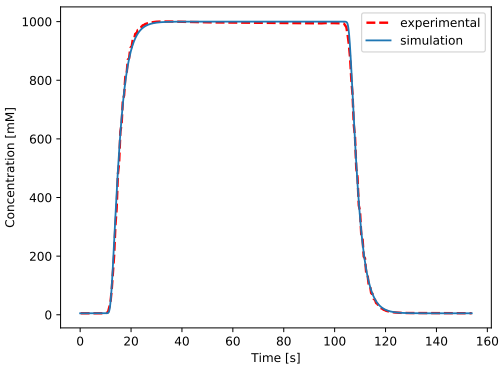

Figure 36: ÄKTA Pilot - Bypass fit for flowrate 100 mL/min

Table 17: ÄKTA Pilot system volumes

PFR length (m)	CSTR 1 (mL)	CSTR 2 (mL)
0.7	5	2

4.3.4 Bubble Trap Model

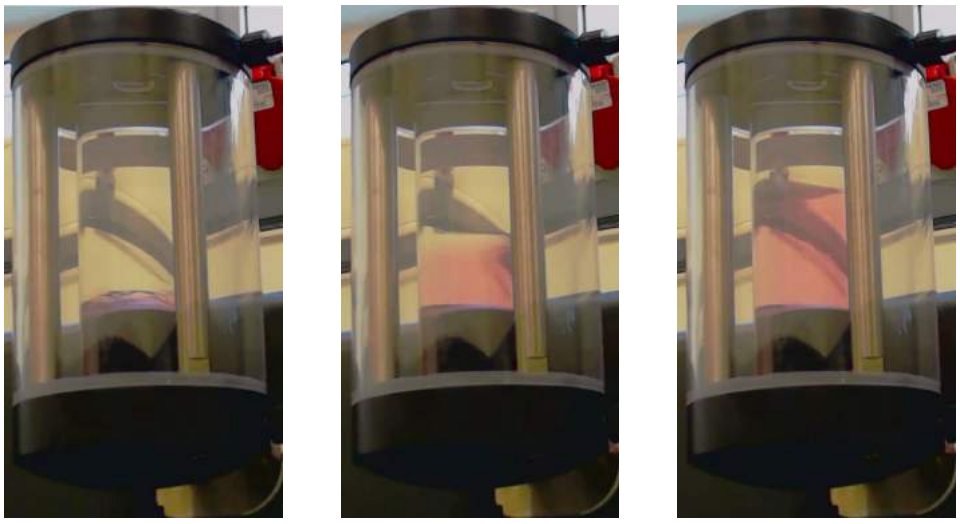

(a) 100 mL/min (b) 200 mL/min (c) 300 mL/min

Figure 37: Mixing volume in bubble trap at different flow rates

The built-in bubble trap of the ÄKTA Pilot system consists of a glass cylinder with an inlet entering a few centimetres above the bottom and an outlet perpendicular to the bottom tank wall. Bubbles traveling with the buffer float to the top of the cylinder and are trapped there.

20mM Tris/HCl 1M NaCl buffer was mixed with vitamin B12 to visualize the mixing behavior inside the bubble trap. A camera was set up to record the mixing and washout behavior during a salt step input at different flow rates. Figure 37 shows the relationship between the mixing volume inside the bubble trap and the applied flow rate. A distinctive boundary between the high-salt buffer and the running buffer can be discerned. The density difference impacts the mixing behavior inside the bubble trap. Furthermore it was determined, that when the valve switches to pure elution buffer the washout is very fast. It is likely that the density difference of the fluids is the cause for this seemingly gravity-assisted washout behavior.

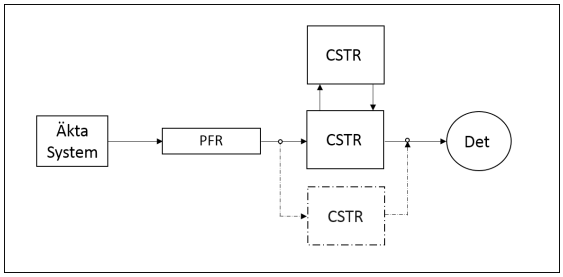

Figure 38: Model of bubble-trap

The observations made based on the video recording lead to the model in Fig. 38, which was developed in cooperation with the CADET development team in the research centre Jülich.

Figure 38 shows the final two-compartment model consisting of three CSTRs. The mixing inside the bubbletrap during the step input is modeled by one CSTR on the bottom connected to a CSTR and the outlet. The percentage of flow split between the two CSTRs was chosen by manual simulation with CADET to match the shape of the transition curve. The final value was chosen as 20% of the system flow. It is likely, that this is density dependent, since a lower density would result in increased mixing between the two sections of the bubble trap. Most of the volume is not mixing with the volume in the top CSTR.

The second part of the model, represented by a dashed line in Fig. 38, describes the rapid washout of the salt by the low molarity buffer. After switching to the low molarity buffer the model changes to a single CSTR which is able to approximate the fast decrease of high molarity buffer in the bubble trap. The volumes of all CSTRs were fitted using CadetMatch for flowrates of 100, 200 and 300 mL/min.

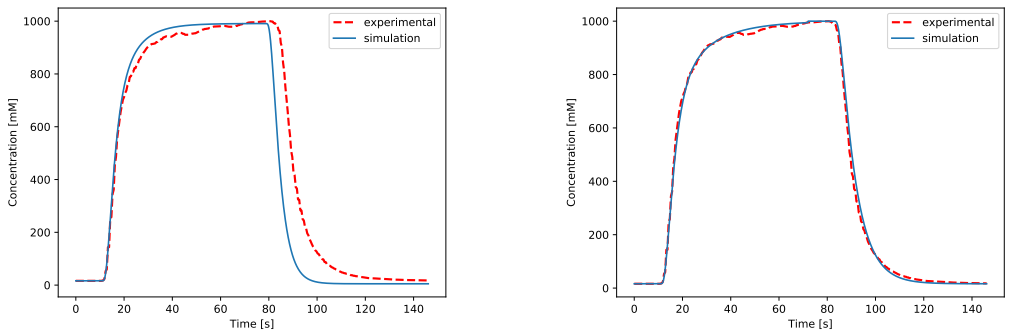

(a) before fitting

(b) after fitting

Figure 39: Bubble-trap simulations at a flow rate of 200 mL/min

Figure 39 shows that fitting the salt transition curve is possible using the bubble-trap model shown in Fig. 38. The fitting process of CadetMatch resulted in a multitude of

Table 18: Parameter optimization results - Volumes of Bubble-trap model

Flow rate (mL/min)	CSTR 1 (mL)	CSTR 2 (mL)	CSTR 3 (mL)
100	11.7	3.9	11.4
200	14.9	7.7	21.5
300	27.7	4.7	34.7

parameter sets ranked by the in-built scoring system. Choosing an appropriate set is not only based on the score. It has to be confirmed by visual examination of the curve shape and position and evaluating the feasibility of the values compared to the physical dimensions of the components on the ÄKTA Pilot system.

4.3.5 Prediction of elution with increased sample load

Forward simulations for increased sample loading and subsequent linear gradient elution were performed using the 6 mL column model in CADET. Fit 1 parameters were used to generate all simulations. Sample load in mg protein / mL column was calculated using the concentration of the simulated BSA monomer solution times the loading time, which was then converted using the molecular mass of monomeric BSA. The simulated column was loaded for the respective times, the column was washed to remove potentially unbound monomer. Next, a LGE was started with a theoretical slope equal to a gradient length of 10 CV. The simulated runs were then reproduced experimentally on the physical equivalent to the programmed column.

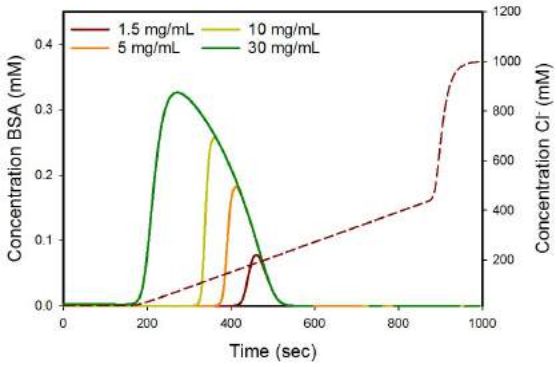

Figure 40: Simulated BSA monomer elution profiles with increasing sample load, gradient length 10 CV

Figure 40 shows, that, according to the simulation, the peaks should elute earlier with an increase in applied sample. The simulation includes protein transport through the pore and the column, the sample load is thus calculated under flow including all protein

and column characterstics including the adsorption model. The monomer moves past sections where there is no unbound ligand left until the whole column is saturated. The simulated column was completely saturated with BSA monomer at a sample load of 30 mg/mL column. Monomer elutes before NaCl leaves the colum, because the monomer which is moving from the top to the bottom of the column propagates a displacement effect throughout, which forces the adsorbed monomer to the outlet of the column. If the mechanistic model is correct the same effect should be observed in the experimental runs.

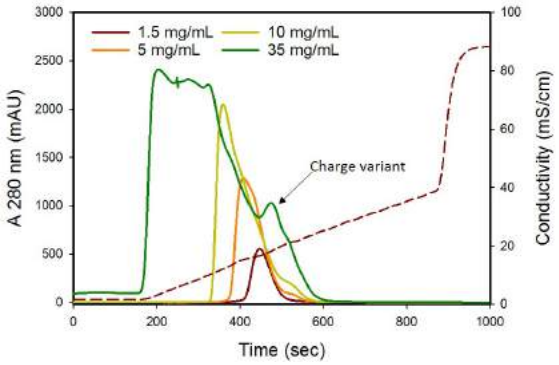

Figure 41: Experimental BSA monomer elution profiles with increasing sample load, gradient length 10 CV

Figure 41 shows the similarity between simulated and experimental elution profiles. Simulations using the modelling described in previous sections are capable of predicting the behavior during increasing sample loads, up to the saturation limit. Interestingly, at higher sample loads, there is separation between the BSA monomer and a seemingly more negatively charged charge variant, whose presence was already suspected during previous experiments, but not as clearly observed.

Comparing prediction and experimental runs shows a discrepancy in the maximum binding capacity of ~ 5 mg monomer per mL column volume, which suggests an inaccuracy in the column model. This could be caused due to a wrongly determined total ionic capacity, particle porosity, or void fraction. Adjustments can be made, but they will change the effect of the previously determined model parameters and a new parameter optimization would have to be performed.

5 Discussion and Outlook

5.1 Discussion

Obtaining equilibrium conditions of mixtures containing aggregates was shown to be complicated by displacement of the monomeric BSA by dimers. This could also be the case for mixtures of other proteins, which would lead to difficulties in estimating model parameters for the SD or SMA model and a larger q_m than for the pure monomer.

Extra-column effects in small columns were shown to have a large influence on the outcome of retention factor determination. Accurate estimation of the dead volume between detectors is paramount in estimating the correct peak salt concentration. The reduced peak salt concentrations at the various gradient slopes prohibit accurate estimation of retention for steep gradients. The peak salt concentration would be drastically underestimated for larger columns. The calculated retention factors vary with column size.

There was no observed influence of the ÄKTA Pilot bubble-trap on LGE. However, performing step elution using the bubble-trap resulted in a higher variance and peak width at base. A model for the mixing behavior inside the bubble-trap was created.

It was found that SMA model parameter determination is not consistent between different methods, e.g. batch adsorption isotherm fitting and CADETMatch fitting of LGE runs. Isotherm data fits differ drastically from values derived from mechanistic model-based fitting. The physical interpretation upon which the SMA model is based is undoubtedly useful for representation of the process occurring in the column, but constricting the model fit by limiting the degrees of freedom, based on this physical interpretation resulted in rather large deviations when compared to other publications[4, 26, 31, 35]. If accurate forward simulations are desired, then, as discussed in [35], the physical feasibility of a parameter is less important than the simulation result, even though the parameters are not congruent with physical properties, e.g. for total ionic capacity. Based on the publications mentioned above, a modeling approach with more variables available for fitting results in a parameter set, which is, even if not physically possible, still valid for performing simulations.

5.2 Further investigation into adsorption behavior

Verification of the displacement process during batch adsorption will be done by a batch kinetic assay. Samples will be taken at defined intervals and the composition of the supernatant will be analyzed by SEC. This should verify the time-dependent displacement of the monomer by the dimer.

5.3 Proposed improvement of fitting strategy for extra-column band-broadening effects

As mentioned in Section 2.6 pre-column band broadening is neglectable for the sample loading step in IEX chromatography of a protein with a rectangular isotherm. However, if a step input is applied to elute the protein, then the shape of the salt transition curve has to be accurately predicted to simulate the appropriate peak shape eluted from the column. This is evidenced by the step elution experiment performed on the ÄKTA Pilot system. A two-pronged approach to model the complete system may be employed to include these requirements into the CADET model. First the system, including a zero volume column is constructed with DPFR and CSTR unit operations to model the pre- and post-column conditions of the system. Then a step input with a salt solution is performed to determine the dimensions of the model that account for the salt transition curve shape as laid out in Section 3.2.11. Here it is important to choose sensible values for the components that cannot be measured with a ruler. The axial dispersion coefficient for the salt is determined for the DPFR units by fitting the transition data. This can be done separately with one tubing with a length of the sum of all the system tubings to generate one value for the tubings. Similar approaches to system modeling were published recently [26, 27].

Protein band broadening occurs only in the column and the post-column volume, hence a protein pulse can be used to determine the axial dispersion in the tubings post-column, by injecting directly into the post-column tubing leading to the UV detector. Then a column can be programmed inserted and the fitting of the column dispersion can be done for both the salt and the protein in turn. This procedure should in theory result in a more accurate modeling of extra-column band broadening contributions for LGE runs.

Acronyms

GRM	General Rate Model
SMA	Steric Mass Action
SD	Stoichiometric Displacement Model
SEC	Size Exclusion Chromatography
CADET	Chromatography Analysis and Design Toolkit
IEX	Ion Exchange Chromatography
AIEX	Anion-exchange
CEX	Cation-exchange
ODE	Ordinary Differential Equations
PDE	Partial Differential Equation
SDS-PAGE	SDS Poly-Acrylamide Gel Electrophoresis
CSTR	Continously Stirred Tank Reactor
PFR	Plug Flow Reactor
DPFR	Dispersive Plug Flow Reactor
BSA	Bovine Serum Albumin
LGE	Linear gradient elution
LFR	Laminar Flow Reactor
PBS	Phosphate-buffered saline
HPLC	High-Performance Liquid Chromatography
EMG	Exponentially Modified Gaussian
RTD	Residence Time Distribution
HETP	Height Equivalent to a Theoretical Plate
SPEA2	Strength Pareto Evolutionary Algorithm 2

Nomenclature

C	concentration in mobile phase, mol m^{-3}
c	concentration in pore fluid, mol m^{-3}
C_0	starting concentration, mol m^{-3}
C_M	peak salt concentration, mol m^{-3}
D_{ax}	axial dispersion coefficient, m^2 sec^{-1}
d_c	column diameter, m
D_e	effective pore diffusivity, m^2 sec^{-1}
d_p	particle diameter, m
k'_i	retention factor for solute
k'_M	retention factor for salt ($=\phi\varepsilon_p$)
K_e	IEX equilibrium constant
k_f	film mass transfer coefficient, m sec^{-1}
L	column length, m
Q	volumetric flow rate, m^3/sec
q	concentration of solute adsorbed on stationary phase, mol m^{-3}
q_0	total ionic capacity of IEXresin, mol m^{-3}
q_{max}	maximum adsorbed solute concentration on stationary phase in SD and SMA adsorption isotherm, mol m^{-3}
q_m	maximum adsorbed solute concentration on stationary phase in Langmuir adsorption isotherm, mol m^{-3}
Sh	Sherwood number
t_G	gradient length, sec
u	linear flow velocity, m sec^{-1}

V	Volume, m^3
v	interstitial flow velocity, m sec^{-1}
z	protein effective charge or net surface charge

Greek Symbols

β	gradient slope, mol m^{-3} sec^{-1}
δ	normalized linear gradient slope, mol m^{-3}
ϕ	phase ratio $(=(1-\varepsilon)/\varepsilon)$
ϕ_{app}	apparent phase ratio, adjusted ϕ for small columns
σ	shielding coefficient in SMA model or standard deviation parameter for Gaussian peak width
τ	dimensionless time
ε	void fraction
ε_b	total bed porosity
ε_p	particle porosity

References

1. Walsh, G. Biopharmaceutical benchmarks 2014. *Nature Biotechnology* **32,** 992–1000 (2014).
2. Gronemeyer, P., Ditz, R. & Strube, J. Trends in upstream and downstream process development for antibody manufacturing. *Journal of Bioengineering* **1,** 188–212 (2014).
3. Carta, G. & Jungbauer, A. *Protein chromatography: process development and scale-up* (John Wiley & Sons, 2010).
4. Kumar, V. & Rathore, A. S. Mechanistic Modeling Based PAT Implementation for IonExchange Process Chromatography of Charge Variants of Monoclonal Antibody Products. *Biotechnology Journal* **12,** 1700286 (2017).
5. Sternberg, J. Extracolumn contributions to chromatographic band broadening. *Advances in Chromatography* (1966).
6. Kirkland, J., Yau, W., Stoklosa, H. & Dilks C.H., J. Sampling and extra-column effects in high-performance liquid chromatography; influence of peak skew on plate count calculations. *Journal of Chromatographic Science* **15,** 303–316 (1977).
7. Hahn, R. Methods for characterization of biochromatography media. *Journal of Separation Science* **35,** 3001–3032 (2012).
8. Gritti, F., Felinger, A. & Guiochon, G. Influence of the errors made in the measurement of the extra-column volume on the accuracies of estimates of the column efficiency and the mass transfer kinetics parameters. *Journal of Chromatography A* **1136,** 57–72 (2006).
9. Kaltenbrunner, O., Jungbauer, A. & Yamamoto, S. Prediction of the preparative chromatography performance with a very small column. *Journal of Chromatography A* **760,** 41–53 (1997).
10. Schweiger, S. & Jungbauer, A. Scalability of pre-packed preparative chromatography columns with different diameters and lengths taking into account extra column effects. *Journal of Chromatography A* **1537,** 66–74 (2018).
11. Yamamoto, S., Nakanishi, K., Matsuno, R. & Kamikubo, T. Ion exchange chromatography of proteinsprediction of elution curves and operating conditions. I. Theoretical considerations. *Biotechnology and Bioengineering* **25,** 1465–1483 (1983).
12. Yamamoto, S., Nakanishi, K., Matsuno, R. & Kamijubo, T. Ion exchange chromatography of proteinspredictions of elution curves and operating conditions. II. Experimental verification. *Biotechnology and Bioengineering* **25,** 1373–1391 (1983).
13. Janson, J.-C. *Protein Purification: Principles, High Resolution Methods, and Applications* (ed Janson, J.-C.) (John Wiley & Sons, 2011).
14. Rosen, J. B. Kinetics of a Fixed Bed System for Solid Diffusion into Spherical Particles. *The Journal of Chemical Physics* **20,** 387–394 (1952).

15. Guiochon, G., Shirazi, D., Felinger, A. & Katti, A. *Fundamentals of Preparative and Nonlinear Chromatography* (Academic Press, 2006).

16. Von Lieres, E. & Andersson, J. A fast and accurate solver for the general rate model of column liquid chromatography. *Computers and Chemical Engineering* **34,** 1180–1191 (2010).

17. Gu, T., Iyer, G. & Cheng, K.-S. C. Parameter estimation and rate model simulation of partial breakthrough of bovine serum albumin on a column packed with large Q Sepharose anion-exchange particles. *Separation and Purification Technology* **116,** 319–326 (2013).

18. Susanto, A., Wekenborg, K., Hubbuch, J. & Schmidt-Traub, H. Developing a chromatographic column model for bovine serum albumin on strong anion-exchanger Source30Q using data from confocal laser scanning microscopy. *Journal of Chromatography A* **1137,** 63–75 (2006).

19. Danckwerts, P. Continuous flow systems: Distribution of residence times. *Chemical Engineering Science* **2,** 1–13 (1953).

20. Langmuir, I. The adsorption of gases on plane surfaces of glass, mica and platinum. *Journal of the American Chemical Society* **40,** 1361–1403 (1918).

21. Kopaciewicz, W., Rounds, M., Fausnaugh, J. & Regnier, F. Retention model for high-performance ion-exchange chromatography. *Journal of Chromatography A* **266,** 3–21 (1983).

22. Brooks, C. & Cramer, S. Steric mass-action ion exchange: Displacement profiles and induced salt gradients. *AIChE Journal* **38,** 1969–1978 (1992).

23. Yamamoto, S., Nakanishi, K. & Matsuno, R. *Ion-Exchange Chromatography of Proteins* (CRC Press, 1988).

24. Schultze-Jena, A., Boon, M., Bussmann, P., Janssen, A. & van der Padt, A. The counterintuitive role of extra-column volume in the determination of column efficiency and scaling of chromatographic processes. *Journal of Chromatography A* **1493,** 49–56 (2017).

25. Kaltenbrunner, O. & Jungbauer, A. Simple model for blending aqueous salt buffers Application to preparative chromatography. *Journal of Chromatography A* **769,** 37–48 (1997).

26. Kumar, V., Leweke, S., von Lieres, E. & Rathore, A. S. Mechanistic modeling of ion-exchange process chromatography of charge variants of monoclonal antibody products. *Journal of Chromatography A* **1426,** 140–153 (2015).

27. Joshi, V. S., Kumar, V. & Rathore, A. S. Optimization of ion exchange sigmoidal gradients using hybrid models: Implementation of quality by design in analytical method development. *Journal of Chromatography A* **1491,** 145–152 (2017).

28. Fogler, H. *Elements of Chemical Reaction Engineering* (Prentice Hall PTR, 2006).

29. Ghosh, P., Vahedipour, K., Leuthold, M. & Von Lieres, E. Model-based analysis and quantitative prediction of membrane chromatography: Extreme scale-up from 0.08ml to 1200ml. *Journal of Chromatography A* **1332,** 8–13 (2014).

30. *CADET - Chromatography Analysis and Design Toolkit Manual -unpublished* (2017).

31. Diedrich, J. *et al.* Multi-state steric mass action model and case study on complex high loading behavior of mAb on ion exchange tentacle resin. *Journal of Chromatography A* **1525,** 60–70 (2017).

32. Zitzler, E., Laumanns, M. & Thiele, L. SPEA2: Improving the strength Pareto evolutionary algorithm. *TIK-report* **103** (2001).

33. Dyson, N. *Chromatographic Integration Methods* X001–X004 (The Royal Society of Chemistry, 1998).

34. Weber, T. W. & Chakravorti, R. K. Pore and solid diffusion models for fixedbed adsorbers. *AIChE Journal* **20,** 228–238 (1974).

35. Osberghaus, A. *et al.* Determination of parameters for the steric mass action model-A comparison between two approaches. *Journal of Chromatography A* **1233,** 54–65 (2012).

36. Wright, M. *An Introduction to Aqueous Electrolyte Solutions* (Wiley, 2007).

37. Hunter, A. & Carta, G. Effects of bovine serum albumin heterogeneity on frontal analysis with anion-exchange media. *Journal of Chromatography A* **937,** 13–19 (2001).